Adam P. Hitchcock

3 Polymer surface characterization by near-edge X-ray absorption fine structure spectroscopy

3.1 Introduction

3.1.1 Scope of chapter

There are many challenges to understanding polymer surfaces and how a specific surface interacts with its surroundings. Such information may be of fundamental interest – *why are some polymer surfaces more hydrophilic than others*? In many cases the properties of a polymer surface are critical for a specific application – *how can the surface of a polymer be made biocompatible and thus suitable for medical applications*? X-ray absorption spectroscopy, and in particular, the near-edge X-ray absorption fine structure (NEXAFS) signal, has much to offer for analyzing polymers and polymer surfaces. In addition to identifying elemental composition, NEXAFS can identify the molecular repeat unit structure, the spatial orientation of functional groups at the surface, the presence and lateral spatial distribution of adsorbates; and how those properties might change under the influence of changes to the physical (T, P) or chemical (e.g., solvent) environment of the surface. This chapter provides an introduction to the principles and instrumentation of NEXAFS, with emphasis on its application to surface-sensitive studies of polymers. NEXAFS microscopy is described. Applications are presented in the areas of organic electronics and biomaterials.

3.1.2 Why NEXAFS?

Tunable monochromatic X-rays are required for NEXAFS spectroscopy. The vast majority of NEXAFS measurements are performed using synchrotron light sources [1], which are large, accelerator-based sources of broad-band electromagnetic radiation (microwave to gamma ray). These facilities have significant barriers to use due to long delays to access, need to travel, remote location, etc. Given the inconvenience relative to home-lab based instrumentation, it is very reasonable to ask, "*why use NEXAFS?*" The short answer is that NEXAFS provides information that is either unique (e.g., polymer orientation at surfaces), or better obtained by NEXAFS than by competing methods. The longer answer can be obtained by reading this chapter.

https://doi.org/10.1515/9783110701098-003

3.1.3 History

NEXAFS is a type of electronic spectroscopy based on the excitation of an inner-shell electron to an energy level or band which is partially of completely unoccupied in the initial state of the sample (typically the ground electronic state). The earliest *soft X-ray* inner-shell spectroscopy to my knowledge was recorded photographically on a number of solids and gases by Hanawalt in 1931 [2]. Hard X-ray (>5 keV) absorption spectroscopy was developed shortly after the discovery of X-rays by Roentgen [3]. However, it was only many years later, after development of improved vacuum, electronics, and optics that systematic studies of soft X-ray absorption spectroscopy began, first using electron energy loss, then monochromated X-rays produced by a synchrotron radiation source. The modern era of inner-shell spectroscopy dates to the mid-1970s when the group of Chris Brion at the University of British Columbia carried out systematic studies of the inner-shell electron energy loss spectra (ISEELS) of many small molecules in the gas phase [4]. Small molecule spectra are of great use in interpreting the NEXAFS spectra of polymers since the ISEEL spectrum of a molecule that is structurally similar to the repeat unit of a polymer is often very close to that of the NEXAFS spectrum of the polymer. My group has continued gas-phase molecular inner-shell spectroscopy studies over the past 40 years. The results have been reported in many papers. A bibliography of atomic and molecular inner-shell spectra and downloadable experimental ISEELS data for over 400 molecules are available at http://unicorn.mcmaster.ca/corex/cedb-title.html.

Synchrotron-based X-ray absorption spectroscopy in the soft X-ray region, which includes the C 1s, N 1s, and O 1s inner-shell spectra that are most relevant to polymer science, also started in the late 1970s [5] but really only emerged as an effective technique with the development of high-resolution monochromators such as the "Dragon"-type spherical grating monochromator [6]. The transition from fundamental studies of atoms and small molecules to studies of solids, surfaces, organic adsorbates on surfaces, and bulk polymers occurred during the late 1970s and early 1980s. That history, along with an excellent exposition of the principles and early applications of NEXAFS, is provided by Joachim Stöhr's excellent book, *NEXAFS Spectroscopy* [7], which, despite being published in 1992, still remains the best monograph dedicated to NEXAFS spectroscopy. An area of application that really brought attention to the power of NEXAFS was studies by the Stöhr group and others of the structure and orientation of small molecules on single-crystal metal surfaces [8]. During the 1980s the first studies of bulk polymers, and then of polymer surfaces were carried out [9–11]. In 1992, Ade et al. reported the first NEXAFS imaging study of a heterogeneous polymer system using scanning transmission x-ray microscopy (STXM) [12].

In addition to Stöhr' book [7], there are a number of excellent reviews of NEXAFS, including ones by Hähner [13] focusing on thin organic films and liquids; DeLongchamp et al. [14] dealing with NEXAFS of molecules and polymers for organic electronics; and Watts et al. [15] providing an excellent summary of physical principles

and experimental methods. Other review articles dealing with applications of NEXAFS to polymers and polymer surfaces include those by Unger et al. [16] comparing NEXAFS and X-ray photoelectron spectroscopy (XPS) as applied to polymer surfaces; Ade and Urquhart [17] outlining the C 1s spectroscopy and microscopy of natural and synthetic polymers; Ade and Hitchcock [18] focusing on NEXAFS microscopy and resonant X-ray scattering of polymers; Son et al. [19] comparing the capabilities of NEXAFS to other spectroscopic techniques for characterizing polymer nanocomposite materials. Fingerprint methods are frequently used in interpreting NEXAFS spectra and thus databases of the NEXAFS spectra of molecules (analogs of polymer repeat units) and polymers are very useful. Dhez et al. [20] reported the spectra of 24 common polymers, organized by functional groups. These spectra can be accessed at https://www.physics.ncsu.edu/stxm/polymerspectro/. Urquhart et al. [21–24] reported the NEXAFS spectra of a number of polyurethanes, polyureas, and polyethers. The review articles by Hähner [13] and Smith et al. [25] contain spectra of many polymers. Graf et al. [26] reported NEXAFS of aliphatic and aromatic amine-terminated polymers in their study of functionalized surfaces. Watts et al. [27] reported calibrated NEXAFS spectra of common conjugated polymers used in organic electronics. Finally, the database of elemental X-ray absorption cross-sections (50 eV to 30 keV), originally published by Henke et al. [28], is an important resource for fundamental properties of X-ray interactions with matter across the whole periodic table. This information is continuously updated and available at the website of the Centre for X-ray Optics (https://henke.lbl.gov/optical_constants/).

3.2 Principles of NEXAFS

3.2.1 Physical processes

When a photon is absorbed by a sample, the photon disappears and its energy is taken up by the internal states of the sample, which, in the X-ray energy regime, involves promotion of an inner-shell (core) electron to an unoccupied level of the target (see Fig. 3.1). Energy is conserved so the absorption will only occur when the energy of the X-ray photon matches the difference in energy of the inner-shell excited state and the ground state. The upper state can be symbolized by (IS^{-1}, U^{1}) where IS is the inner-shell level, U is the unoccupied level and the superscripts indicate that, relative to the ground state, there is one less electron in an IS orbital (e.g., C 1s, the most important inner-shell level in the context of NEXAFS of organic polymers) and there is one more electron in one of the unoccupied orbitals of the ground state (e.g., π^* in a closed shell, unsaturated organic molecule) or partly occupied (e.g., 3d in an open-shell transition metal species). The high-energy excited state created by an X-ray absorption event is very short lived (femtosecond or shorter lifetime) because it rapidly

decays by either X-ray fluorescence radiation or by a non-radiative Auger electron decay (Fig. 3.1). In the radiative X-ray fluorescence process, an electron in one of the occupied, less tightly bound inner-shell or valence (V) orbitals fills the inner-shell hole and emits an X-ray at the same time to conserve energy. In non-radiative Auger decay, two electrons in less tightly bound orbitals are involved, with one filling the inner-shell hole and the other being ejected from the sample. In the soft X-ray region (<1000 eV), the probability of X-ray fluorescence is very low (<1%) and the Auger process dominates. NEXAFS spectra can be acquired in many different modes, which allows adjustment of the spatial sensitivity and other aspects of the method. Thus, if transmission or X-ray fluorescence (FY) detection is used, the spectra reflect the properties of the bulk of the material because X-rays penetrate far into matter (50–1000 nm in the 50 eV to 1 keV range). Various signals involving emitted electrons – drain current (total electron yield, TEY), photoelectron yield (PE-EY), Auger electron yield (AEY), or secondary electron yield (SEY) with a defined energy bandwidth (PEY) – provide variable extents of sensitivity to the sample surface, with the sampling depth dependent on which type of electrons detected. Other channels, such as partial or total ion yield can provide even higher surface sensitivity, while others, such as luminescence or thermal detection, can enhance bulk sensitivity. Lateral sensitivity (NEXAFS microscopy) [29] can be achieved by use of a focused X-ray beam (STXM or scanning photoelectron

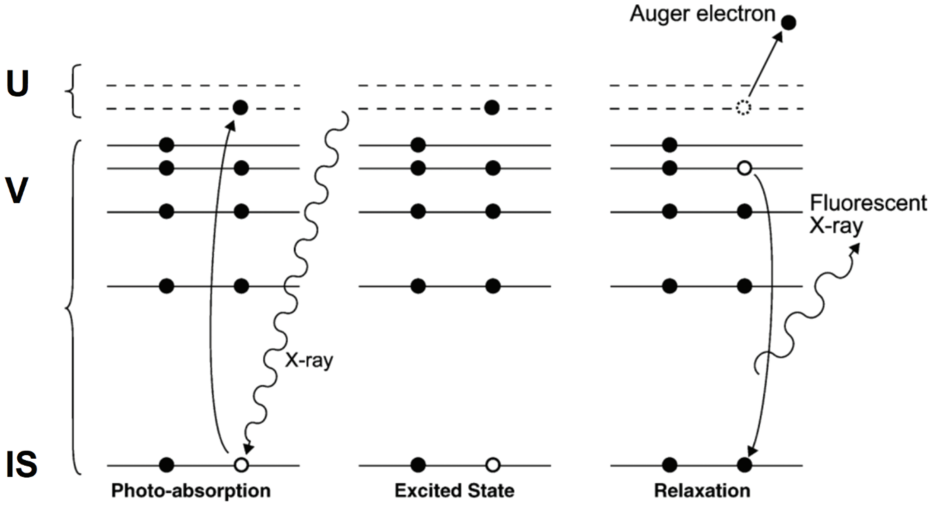

Fig. 3.1: Schematic of the photoabsorption and subsequent relaxation processes involved in near-edge X-ray absorption fine structure (NEXAFS) spectroscopy. A monochromatic X-ray photon is absorbed by the system in a resonant process that excites an electron from an inner-shell (IS) level to an unoccupied (U) level. This creates a highly excited state which rapidly relaxes by an electron in a less tightly bound occupied valence (V) or IS level filling the IS hole, simultaneously ejecting an Auger electron or emitting an X-ray fluorescent photon (adapted from fig. 1 of [15], used with permission).

microscopy, SPEM) or by imaging the spatial distribution of transmitted photons (transmission X-ray microscopy, TXM) or ejected electrons (X-ray photoemission electron microscopy, XPEEM). More details on NEXAFS microscopy are provided at the end of this chapter.

3.2.2 Theory

X-ray absorption and X-ray fluorescence processes are governed by electric dipole selection rules, which in the simplest form, strictly applicable only to atoms, requires a unit change in the orbital angular momentum quantum number, ℓ:

$$\Delta\ell = \ell \pm 1 \tag{3.1}$$

In the context of NEXAFS of polymers, where the C 1s, N 1s, and O 1s edges are most commonly measured, the strongest inner-shell excitations are those which involve promotion of 1s electrons to unoccupied orbitals with a large 2p component on the same atom where the inner-shell excitation took place. The intensity of an X-ray absorption process involving the transition from an initial, |i>, to a final state, |f> is governed by the transition dipole moment (TDM):

$$TDM = <f|e.r|i> \tag{3.2}$$

Since the TDM contains a spatial overlap component and inner-shell (core) orbitals are very compact and centered about a single atom, NEXAFS transitions are spatially localized at the atom whose inner-shell electron is excited. This is true even in the case of species where there are symmetry equivalent atoms, such as ethane, since creating the inner-shell hole breaks the symmetry [30]. Thus, a simplistic but often effective way of estimating 1s excitation intensities is the contribution of 2p atomic orbitals on the inner-shell excited atom to the upper molecular orbital of the transition (i.e. the square of the coefficient for the 2p atomic orbital on the core excited atom to the final molecular orbital). This approach has been used to approximate inner-shell excitation spectra from simple, semi-empirical molecular orbital calculations [31, 32]. More correctly, the inner-shell spectrum can be predicted by quantum chemical calculations in which the energies and wavefunctions of the initial ground state and the final inner-shell excited states are calculated, and used to compute the transition dipole matrix element (eq. (3.2)). Ideally, such calculations should take into account all relevant interactions including relaxation of all energy levels in the presence of the core hole, electron correlation, and the interaction of isolated molecules with their local environment (e.g., an underlying substrate in the context of surface adsorbed species). It is only in recent years that the computational power and sophistication of quantum chemical calculations, particularly density functional theory (DFT) codes, have developed to the level where calculations can accurately predict inner-shell spectra of modestly complex systems [33–35]. The

GSCF3 method [36], an intermediate level of quantum calculation which includes a localized core hole but not electron correlation, has had much success at reproducing energies and intensities of discrete core excitations below the inner-shell ionization limit in many molecular systems [21–24, 37, 38].

3.3 Techniques

3.3.1 Experimental aspects

To date almost all NEXAFS spectra of organic molecules and polymers have been measured using synchrotron radiation. Lab-based spectrometers exist [39] but only recently have they begun to approach the performance of synchrotron systems [40]. Lab systems have not yet had much impact on polymer surface science so they will not be discussed further. Figure 3.2a is a cartoon of a soft X-ray (50–3000 eV) synchrotron radiation beamline that is used for NEXAFS. The X-ray source may be a bend magnet (BM) or (increasingly) an undulator [41]. BM, which guides the electron beam around the storage ring, provides a continuum of X-rays with strong linear polarization in the horizontal plane. Undulators (Fig. 3.2b), a type of insertion device [41], consist of a periodic array of magnets above and below a straight section of the storage ring. These magnet arrays are mounted on moveable rails, which allow tuning the undulator emission. The undulating magnetic field modifies the electron trajectory, and converts the intrinsically broad BM spectrum into a series of narrow, intense peaks of radiation (Fig. 3.2c) [42, 43]. By displacing the magnets vertically (closing or opening the gap), the photon energy is changed. If one of the magnet arrays is shifted along the straight relative to the other array, the relative phasing of the magnets is changed which modifies the direction of linear polarization. If the top and bottom arrays are split so there are four magnet arrays, motion of three of these arrays relative to the fourth allows the user to fully control the polarization of the X-rays: fully circular; fully linear with the electric vector positioned over an angular range of ±180°; and, arbitrary elliptical polarization[42]. Such elliptically polarizing undulators (EPU) provide the largest flexibility and are particularly useful in NEXAFS microscopy [44]. Mirrors are used to focus and redirect X-rays. A grazing incidence diffraction grating is used to disperse the polychromatic X-rays in space. The exit slit selects a specific energy of monochromatic light. By precisely rotating the diffraction grating, a range of photon energies can be scanned while collecting one or more signals sensitive to the X-ray absorption. All parts of the system are in ultra-high ($<10^{-9}$ mbar) vacuum.

A typical synchrotron beamline used for NEXAFS is the soft X-ray beam line and Brookhaven National Laboratory, operated by scientists from the National Institute for Science and Technology (NIST). Originally this was on the UV ring of NSLS-1 [11],

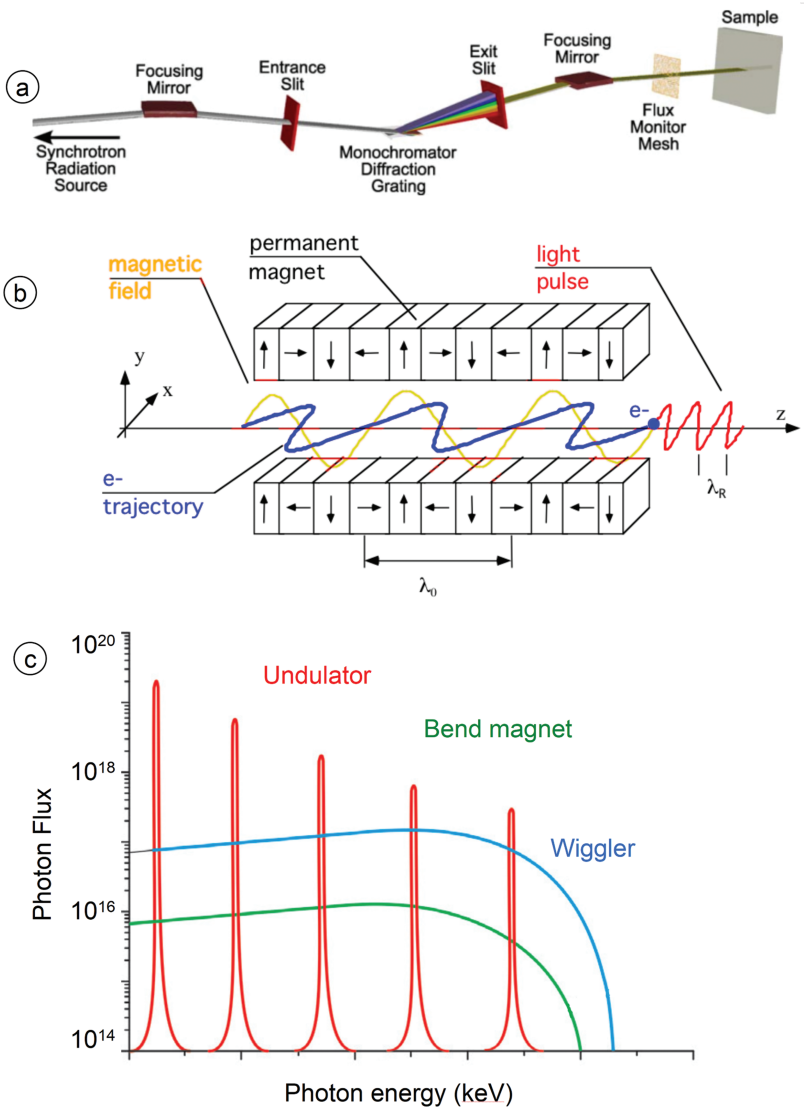

Fig. 3.2: (a) Schematic of a soft X-ray (50–3000 eV) synchrotron radiation beamline. Mirrors are used to focus and redirect X-rays. A grazing incidence diffraction grating is used to spatially disperse the polychromatic X-rays. An exit slit selects a specific energy of monochromatic light. All parts of the system are in ultra-high vacuum ($<10^{-9}$ mbar). (b) Cartoon of an undulator. A periodic array of strong, permanent magnets imposes a sinusoidal motion (wavelength λ_u) of the electron beam in a straight section of the storage ring. The light emitted at each of the N turns in the trajectory reinforces each other in a laser-like fashion, producing a 2N-fold increase in flux and 1/N reduction in the angular spread of the X-ray beam. (c) Multi-harmonic undulator spectrum compared to that of a wiggler and a bend magnet source. (adapted from [43], used with permission).

but it has recently been replaced with a higher performance system, BL 7-ID-1 at the fourth generation source, NSLS-II [45]. Typically synchrotron beamlines are used for a variety of experiments, such as X-ray photoemission (XPS) which has been described in Chapter 2, resonant inelastic X-ray scattering (RIXS), etc., and the portion of beamtime used for polymer studies is limited. In an earlier era, users might even bring their own experimental chamber to synchrotron facilities. These days it is overwhelming the case that the facility builds, commissions, maintains, and evolves the capabilities of both the source (storage ring and beamline) and the experimental end stations. The users (a government, industrial, or academic scientist, often accompanied by postdoctoral fellows and graduate students) are responsible for defining the scientific goals, fabricating samples, bringing them to the beamline, verifying their integrity (e.g., off-line surface conditioning and characterization), operating the system (under supervision of the beamline scientist), analyzing the results and preparing publications. Access to synchrotron facilities is administered through a peer review process which involves proposal submission, review by experts in the field, scoring and beamtime allocation based on those scores. At competitive beamlines, success rates for proposals can be less than 25%, in some cases less than 10% for NEXAFS microscopes. Typically there is a 4 month interval between proposal submission and the period when beam might be allocated. Many facilities provide access for up to 2 years (four 6-month periods) on the same proposal, although some require submission of a new proposal for each 6-month period.

3.3.2 Detection schemes

Figure 3.3a summarizes the most common NEXAFS detection schemes. In general the incident flux intensity will vary with photon energy, and with time, for light sources that operate in decay mode. Increasingly, the light sources are operated in top-up mode, in which the storage ring current is kept constant by frequent small refill procedures. In order to get correct NEXAFS spectra it is necessary to measure the incident intensity (I_o), ideally with the same detector (which is realistically only possible in transmission geometry) or one with a similar spectral response in the energy regime measured [15]. For transmission detection the transmitted intensity (I) and I_o are input to the Beer–Lambert law (see eq. (3.3)) to obtain a valid NEXAFS spectrum. For all yield measurements (TEY, PEY, AEY, FY) the yield signal is divided by the I_o signal.

3.3.2.1 Transmission

When transmission detection is used, the incident (I_o) and transmitted (I) signals are measured, and the NEXAFS spectrum is obtained in the absorbance or optical density (OD) form using the Beer–Lambert law:

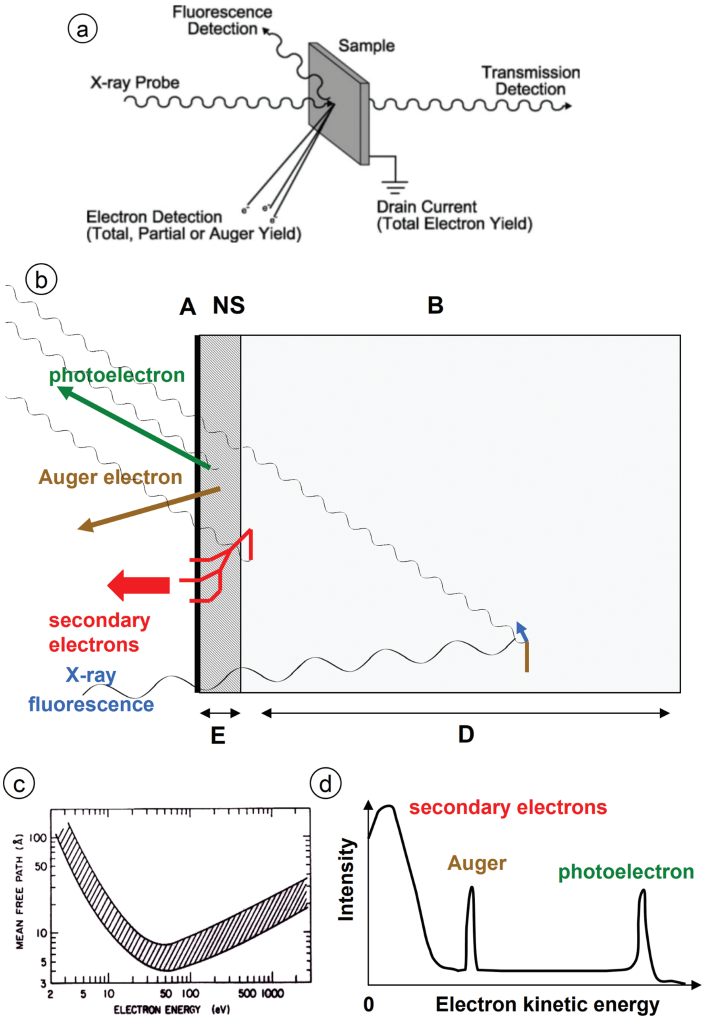

Fig. 3.3: (a) Signals are used to detect NEXAFS. Transmission or X-ray fluorescence if the sample is very thin; various types of energy-resolved electron yield (secondary, photoelectron, Auger); and total electron yield via sample current. (b) Schematic of X-ray–sample interactions. Soft X-ray photons penetrate far into samples – from several hundred nanometers up to a few microns, depending on the X-ray energy and the material. X-ray fluorescence (XRF) photons have a similar range, such that XRF detection will give the NEXAFS of the bulk (B) of the sample. Photoelectrons or Auger electrons can only escape from the near surface (NS), < 2 nm into the sample, and thus are best for detecting absorbates (A). Secondary electrons, usually 5–50 eV kinetic energy, generated by inelastic scattering of photoelectrons or Auger electrons, can escape from zone E, up to 10 nm into the surface, depending on photon energy. (b) Universal inelastic mean free path for electron scattering. (c) Dependence of the inelastic mean free path in solids (distance an electron can travel before an inelastic collision) on the electron kinetic energy. (d) Sketch of a typical kinetic energy spectrum of electrons ejected from an X-ray irradiated sample.

$$\mathrm{OD} = -\ell n\left(\frac{I}{I_0}\right) = \sigma\rho t \tag{3.3}$$

where σ is the photon energy dependent cross-section, ρ is the sample density, and t is the thickness. In order to use transmitted X-rays to measure a NEXAFS spectrum, the sample must have an appropriate thickness, which is optimally that which gives an OD of 1 at the most intense absorption peak. If the sample is too thick, such that the peak OD is above 3, the resulting absorption saturation can greatly distort the shape of NEXAFS spectra. Absorption saturation occurs in thick samples due to contributions from electronic and other sources of backgrounds, and higher order spectral contributions when most of the incident photons are absorbed by the sample [46]. If the sample is too thin, such that the peak OD is less than ~0.1, it is difficult to obtain good statistics.

3.3.2.2 Electron yield methods

In general electron detection methods provide much higher surface sensitivity than photon detection methods (transmission, fluorescence yield). The simplest way to measure the total electron yield is to electrically isolate the sample and measure the drain current between the sample and electrical ground. The drain current is directly related to the number of electrons ejected when the incident X-ray beam hits the sample. The ejected electron current is the sum of electrons from the primary photoionization and Auger decay processes, along with secondary electrons generated indirectly from ionizing inelastic scattering events as the photo-electron and Auger electron travel to the surface (see Fig. 3.3b). The X-ray photon penetration depth (roughly 1 μm per keV) is much larger than the electron escape depth (1–10 nm). The sampling depth (region of the sample contributing to an electron yield NEXAFS spectrum) depends on the kinetic energy of the electrons detected and their inelastic mean free path (Fig. 3.3c) [47, 48]. The primary photoelectron and Auger signals, which have well-defined electron kinetic energies, can only be detected if their kinetic energy is unchanged and thus only come from very near to the surface. The secondary electron signal, especially the low kinetic energy electrons (<20 eV), will come from a much larger range of depths, including several tens of nanometers. In order to measure the primary electrons with well-defined kinetic energy, an electron energy analyzer and a high, or ultrahigh vacuum system are required. TEY and PEY methods can be done in a low vacuum ($<10^{-3}$ mbar) using retarding grids and a suitable electron detector such as a photodiode, a channeltron, or a channelplate, combined with appropriate electronics. For all types of electron yield detection, sample charging in the case of insulating samples can be an issue. In such cases, a very thin coating of a conducting material (e.g., Pt) can be used, although that may compromise the polymer surface chemistry of interest. Charging is worst for the primary electrons

since PE-EY and AEY detection modes require stable, well-defined kinetic energies. PEY and SEY are relatively tolerant to some charging, while transmission and XRF modes are immune to sample charging.

3.3.2.3 Photon yield methods

X-ray absorption can be measured by detecting X-ray fluorescence photons, as either a total fluorescence yield or partial fluorescence yield (PFY). While FY is very important for studies of the bulk of solids, especially at higher X-ray energies where the fluorescence yield is high, it is rarely used for surface studies in the soft X-ray regime, in part due to the very low fluorescence yield from core edges below 1000 eV. Situations where FY detection has been used to advantage is in the study of organic polymers that are part of another material that did not contain carbon, with the polymers either as a thin coating on the surface, or as a thin layer that is buried at a depth less then the escape depth of the C Kα X-ray fluorescence photon (260 eV), about 300 nm [13, 49]. Simultaneous acquisition of the polarization dependent electron yield (TEY or SEY) and FY spectra are often used to compare properties of the surface and bulk of a polymeric material, in terms of both composition and molecular orientation [50, 51]. If the fluorescence X-rays are detected with an energy resolving detector such as a silicon drift detector, further options become available, including selective detection of minority elements in a polymer (e.g., S in thiophene-containing organic photovoltaic materials [52]) and use of inverse PFY which reduces the distortions from absorption saturation of fluorescent X-rays by too thick material [53]. In general, although the C Kα fluorescence yield is very low (<0.1% of the decay of C 1s core holes), the ever increasing brightness and stability of modern synchrotron light sources tends to compensate for the low fluorescence yield, although radiation damage can be a limiting factor on high flux beamlines, and especially in NEXAFS microscopy where the focused X-ray beam can deliver a very large radiation dose [29, 48].

3.3.3 Surface-sensitive detection

If the element of interest is localized at the surface and the underlying material does not contain that element, then any NEXAFS detection method may suffice since inner-shell edges are widely spaced. However, in order to be sensitive to the very surface – defined as one monolayer – a detection method that has a very shallow escape depth is needed, especially if the goal is to differentiate the structure/composition of the very surface from underlying layers which have the same or a similar composition. Among the methods described above, PE-EY and AEY are the most surface sensitive. It is also possible to enhance surface sensitivity by using ions ejected from the

surface as the detection channel, either as a total ion current (TIY), or with mass spectrometric detection of individual mass-resolved ions (PIY) [54]. However the ion signal is weak, due to recapture of ions at the surface. Also, since soft X-rays penetrate hundreds of nanometers into the sample, energetic electrons (photoelectrons, Auger, secondary) can ionize atoms in the near-surface region, thereby mixing and often overwhelming the surface-specific signal with a spectral signature characteristic of regions much deeper into the sample [55]. Another way to enhance surface sensitivity is to tilt the sample and use a grazing incidence X-ray beam. This will reduce the penetration depth of the photons, and increase the contribution from X-ray absorption in the surface region. However, given that a 300 eV photon penetrates on the order of 500 nm, an angle of ~1° (~0.1°) is needed to reduce the penetration to ~10 (1) nm. If the width of the X-ray beam is 100 μm (a typical beam size for spectroscopy synchrotron beamlines) the lateral spread of the beam on the surface will be 5 mm at 1° incidence and 50 mm at 0.1° incidence.

3.4 Interpreting NEXAFS spectra

3.4.1 Common features of a NEXAFS spectrum

The energy of an inner-shell spectral feature will depend on the energies of both the core level and the ground state unoccupied level to which the electron is excited. The core-level energies, which are essentially those detected in X-ray photoelectron spectroscopy (XPS) (see Chapter 2) are determined by the local environment, with the main factor being the electronegativity of the atoms directly attached to the atom where the core excitation takes place. Thus the C 1s level in aliphatic polymers (only C–C and C–H single bonds) are ~ 285 eV. When carbon is bound to electronegative atoms the C 1s core-level binding energy (BE) shifts to lower energy. Thus the C 1s BE of $\underline{C}$–O carbons is ~ 286 eV, that of $\underline{C}$ = O carbons is ~ 289 eV, that of $\underline{C}$–F is ~ 289 eV, that of $\underline{C}F_2$ is ~ 292 eV and that of $\underline{C}F_3$ is ~ 294 eV [56]. The unoccupied levels of the ground state, which are the upper level of the transition, are quite sensitive to the chemical environment and thus the fine details of a NEXAFS spectrum reflect the molecular structure. Typically the strongest NEXAFS features are those involving excitations to compact valence-type levels which have large 2p density on the core excited atom. For organic polymers these are π* levels for unsaturated species, and σ* levels for both unsaturated and saturated species. The 1s → π* transitions tend to be sharp and at lower energy; they are usually the spectral features used for qualitative identification (see Fig. 3.4). The 1s → σ* transitions occur at somewhat higher energy. For σ* features associated with bonds between second row atoms (B – F), there is a correlation between term values (difference in energy of the 1s → σ* transition and the 1s

binding energy) and bond lengths [57], which can be used for spectral assignment and compound identification.

Detailed assignment and understanding of all the details of the spectrum of a specific molecule or polymer requires accurate quantum mechanical calculations of the electronic states of the molecule (see Section 3.2.1). However in many cases the spectra can be adequately understood by comparison to small molecules with a structure similar to that of a polymer – for example, ethane as a model for polyethylene. In general additivity principles apply – for example the C 1s spectrum of phenylalanine is quite accurately simulated by the sum of the C 1s spectra of benzene and alanine [58]. In addition, when there are characteristic functional groups, such as pendant phenyl groups, nitrile or carbonyl groups, these tend to have transitions at similar energies in all molecules. Finally, by recording the NEXAFS spectra of reference materials, fingerprinting identification methods can be used.

3.4.2 Polymer NEXAFS – fingerprinting and functional group identification

Figure 3.4 presents a montage of C 1s NEXAFS spectra of a range of polymers. While a detailed analysis of each spectrum can and has been done for most of these spectra, the main message of this figure is to show that the C 1s spectra of even chemically closely related polymers – e.g., polystyrene (PS) and brominated polystyrene (PBrS) – are readily differentiated. This means that NEXAFS can be used in a fingerprint fashion by comparing the spectrum of an unknown polymer to a data base of polymer spectra (e.g., https://www.physics.ncsu.edu/stxm/polymerspectro/). While NEXAFS of closely related species can be differentiated, there are many similarities for polymers containing the same functional groups. For instance, all polymers containing a phenyl group have a sharp intense C 1s $\rightarrow \pi^*$ peak around 285 eV, ester groups have a prominent C 1s $\rightarrow \pi^*_{C=O}$ peak at 285.4–285.6 eV, etc. Figure 3.5 summarizes the energy ranges where different functional groups are typically found. Within the class of carbonyl species (aldehydes, ketones, amides, esters, ureas, urethanes, carbonates, etc.), the sensitivity of NEXAFS to the type of carbonyl species rivals that of infrared spectroscopy [59].

3.4.3 Linear dichroism – theory

This is one of the most important and widely used properties in synchrotron-based NEXAFS studies of polymer surfaces. In the following, the X-rays are assumed to be 100% linearly polarized, as can achieved with undulators [43]. Bend magnet beamlines typically have only 85% linearly polarized light [7, 11]. That reduced degree of polarization must be taken into account in quantitative analyses of angle-dependent

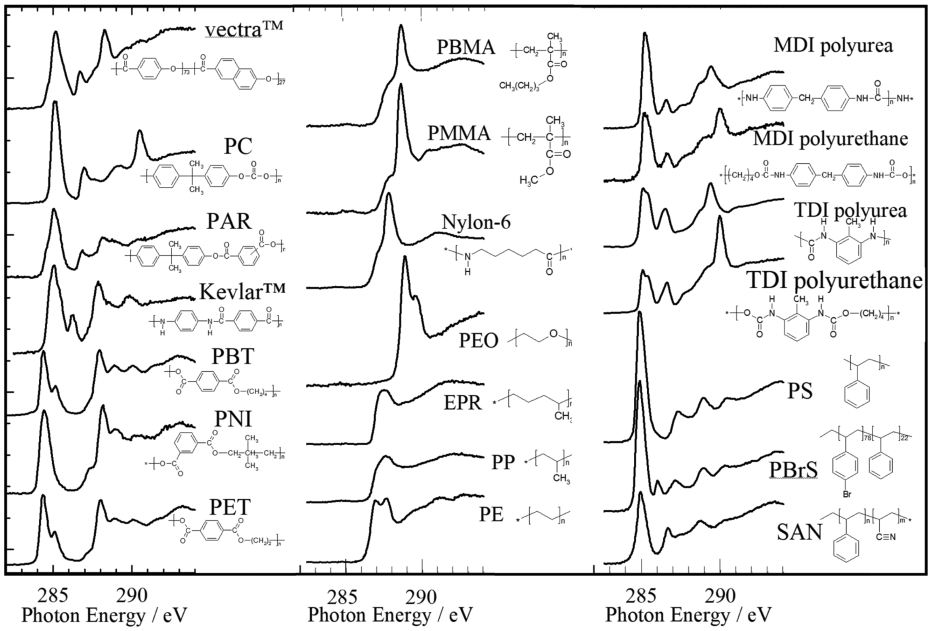

Fig. 3.4: C 1s NEXAFS spectra of 21 different polymers showing the capability of NEXAFS for identification and chemical analysis of polymers (composite of data reported in references [20–25]).

NEXAFS studies. The intensity of a NEXAFS transition is related to the square of the electric dipole transition matrix element (TDM, eq. (3.2)). The angular distribution of the intensity of each transition is governed by the symmetry properties of the TDM and its orientation relative to the electric vector ($\underline{E}$) of the incident X-rays [7, 60]:

$$I\alpha|E.\langle f|\mu|i\rangle|^2\alpha\cos^2\theta \tag{3.4}$$

where θ is the angle between the electric vector ($\underline{E}$) and the direction of the TDM. The following treatment is restricted to excitations of electrons from 1s orbitals, since C 1s, N 1s, and O 1s are the most important edges for organic polymers. For a 1s initial orbital and a directional final orbital, $\underline{O}$, the matrix element $|\underline{E}.<f|\mu|1s>^2$ points in the direction of the final orbital $\underline{O}$ and the transition intensity becomes

$$I\ \alpha\ |E.\langle f|\mu|i\rangle|^2\ \alpha\ |\underline{E}.\underline{O}|^2\ \alpha\cos^2\theta \tag{3.5}$$

In general, 1s excitations have the highest intensity when the 2p component of the unoccupied orbital to which the 1s electron is excited is aligned along the electric vector of the linearly polarized X-rays. Thus, for a monolayer of benzene that is adsorbed on a Ag(110) surface, where the plane of the molecule is parallel to the surface, the intensity of the C 1s → π* transitions are greatest when measured with

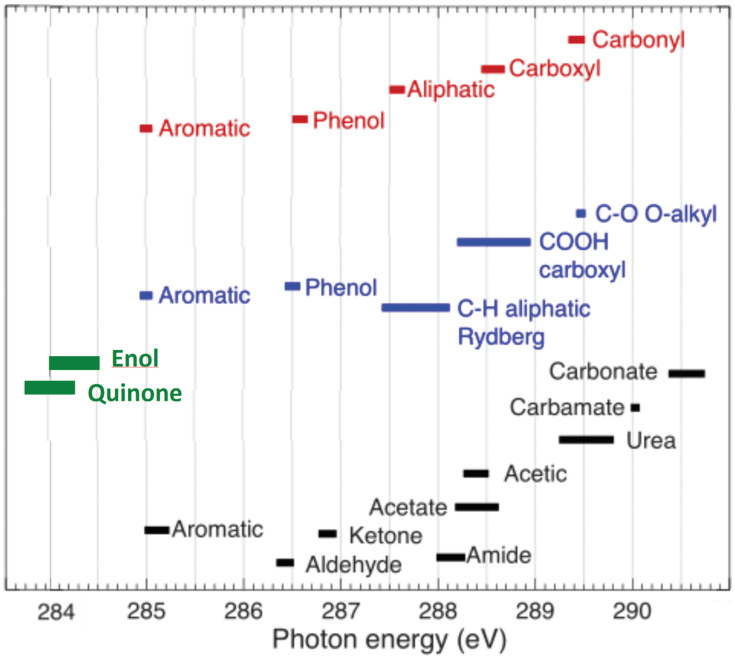

Fig. 3.5: Energy ranges for characteristic, mostly C 1s → π*, transitions of different functional groups, including carbonyl compounds (black) [59], enol and quinone compounds (green) [102, 103], and organic components of soils (blue [104, 105] and red [106]).

grazing incidence X-rays (where the *E*-vector is nearly perpendicular to the surface) and weakest when measured with normal incidence X-rays (where the E-vector is parallel to the surface) [61, 62] (see Fig. 3.6). In contrast C 1s → σ* transitions are strongest at normal incidence (where the *E*-vector is in the plane of the benzene ring, as are the σ* orbitals), and weakest at grazing incidence [61, 62]. While this example illustrates the concept of using NEXAFS linear dichroism to qualitatively determine molecular orientation at a surface, the real power of NEXAFS linear dichroism comes from a quantitative analysis of how the intensity of a specific NEXAFS transition varies with systematic changes in the angle between the *E*-vector and the sample [63]. Both polar and azimuthal tilting can be used. A detailed geometric approach describing 1s excitation to specific unoccupied orbital shapes (linear, vector, and planar) and involving four separate angles was developed by Stöhr [7]. A symmetry analysis [63–65] is conceptually simpler, and also treats the most general cases, including excitation from p, d, and f inner-shell levels.

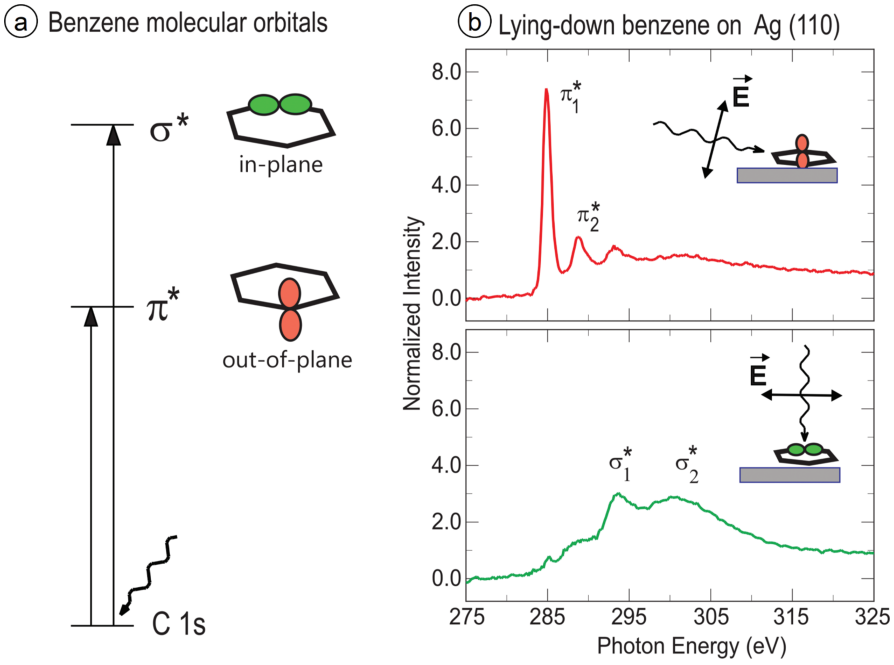

Fig. 3.6: (a) Schematic of inner-shell excitations to the unoccupied π* and σ* energy levels that dominate the NEXAFS spectra of benzene. (b) Polarization dependence of the C 1s NEXAFS spectrum of a monolayer of benzene on a Ag(110) surface where the molecule adsorbs with the molecular plane parallel to the surface [62]. C 1s → π* excitations are most intense when the electric vector of the X-rays ($\vec{E}$) is perpendicular to the plane of the ring. C 1s → σ* excitations are most intense when $\vec{E}$ lies in the plane of the ring (used with permission, private communication).

3.4.4 Linear dichroism – examples

Figure 3.7 shows an example of a linear dichroism study of the C 1s NEXAFS of a thin film of polytetrafluoroethylene (PTFE) on a silicon wafer, aligned parallel to the surface by gently rubbing a piece of PTFE across the Si surface which had been heated to 150oC [66]. These PEY NEXAFS spectra were recorded using X-rays at normal incidence ($\underline{E}$ parallel to the surface) and at grazing (20°) incidence ($\underline{E}$ almost perpendicular to the surface). The C 1s → σ^*_{C-C} transition at 286 eV is most intense in the normal incidence spectrum, which is consistent with the $-(CF_2-CF_2)-$ chains lying parallel to the surface. The C 1s → σ^*_{C-F} transitions at 292 and 299 eV are most intense at glancing incidence but have some intensity at normal incidence. Detailed analysis of the polarization dependence, assisted by calculations, showed these polarization-dependent NEXAFS spectra were consistent with a 13/6 helical conformation (6 turns in 13 repeat units), and not consistent with other helical structures or a zigzag conformation known to exist at high pressure [66].

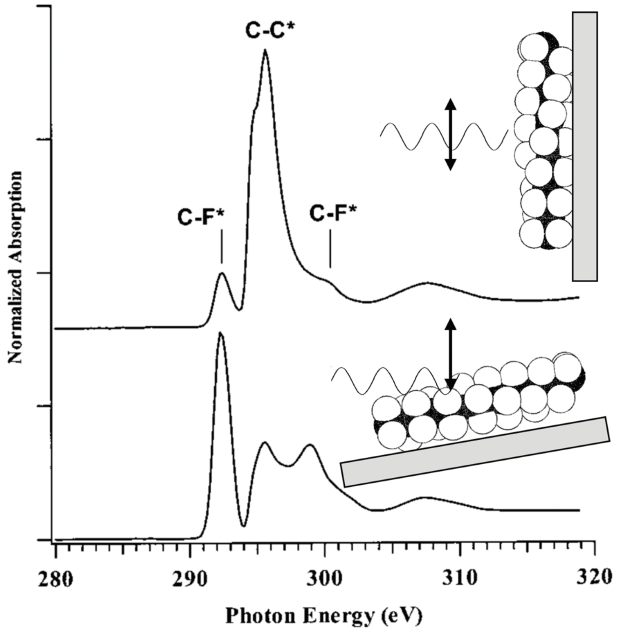

Fig. 3.7: (a) C 1s NEXAFS of an oriented thin film of polytetrafluoroethylene (PTFE) on a Au-coated Si wafer, recorded with the X-rays at normal incidence ($\vec{E}$ parallel to the surface) and grazing (20°) incidence ($\vec{E}$ almost perpendicular to the surface [59]. The C 1s → $\sigma^*_{C\text{-}C}$ transition (286 eV) is most intense in the normal incidence spectrum which is consistent with the –(CF_2–CF_2)– chains lying parallel to the surface in the indicated 13/6 helical conformation. The C 1s → $\sigma^*_{C\text{-}F}$ transitions (292 and 299 eV) are most intense at glancing incidence but have intensity at normal incidence. Detailed analysis of the polarization dependence, assisted by calculations, showed the NEXAFS data was consistent with a 13/6 helical conformation (13 advances for 6 turns of the helix), and not consistent with tighter (7/6) or looser (19/6) coiled configurations, or with a zigzag conformation known to exist at high pressure (adapted with permission from fig. 1 of [66]. Copyright 2002, American Chemical Society).

Figure 3.8 presents results of a NEXAFS polarization study of an annealed 50 nm thick pentacene thin film which is a material used in organic thin film transistors (OTFT) [11, 14]. The results display a very systematic variation of the intensities of the NEXAFS features with the angle between the $\underline{E}$-vector and the sample. Notably, the low lying C 1s → π* spectral features at 284.2 and 285.8 eV increase in intensity when the orientation of the X-ray beam relative to the surface approaches normal incidence while the σ* features at 294.9 and 301 eV increase in intensity when the incident X-ray direction approaches glancing incidence. Thus, the π* orbitals are preferentially oriented in the substrate plane, and the pentacene molecules are oriented edge-on in the thin film. The π* variation indicates only the orientation of the conjugated plane. It cannot be used to determine the orientation of the long axis of the pentacene (see insert to Fig. 3.8b). For that, the dichroism of the σ*

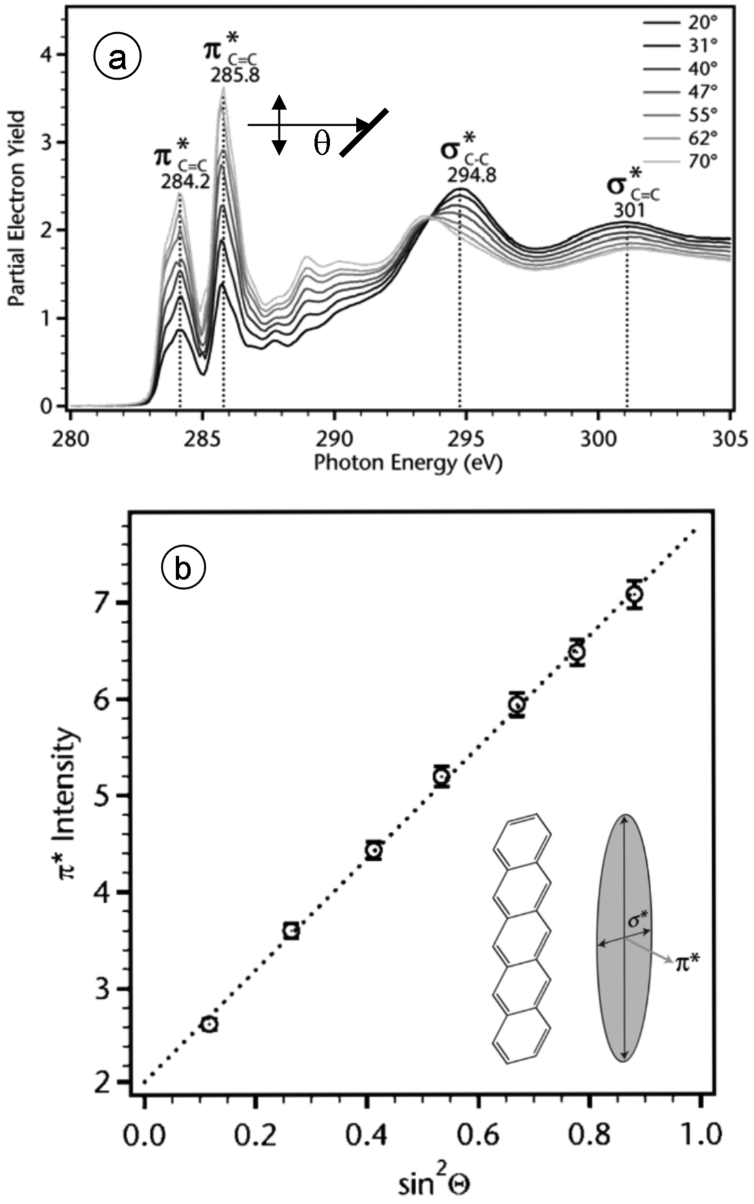

Fig. 3.8: Pentacene C 1s NEXAFS dichroism. (a) C 1s spectra of a free-standing 50 nm thick pentacene film, that was highly oriented by deposition on a Si wafer followed by annealing [11]. (b) Plot of the integrated C 1s → π* intensity (282–286.5 eV) versus $\sin^2 \theta$, where θ is the angle between the surface and the X-ray beam. The inset figure indicates the orientational vectors of the in-plane σ* and out-of-plane π* orbitals which are the terminus of the C 1s excitations (adapted from [11], used with permission).

resonances is used. The σ* intensity is most intense near glancing incidence, where the electric field vector is normal to the substrate plane. Thus, the long axis of the σ* ellipse is preferentially normal to the substrate, and the long axis of pentacene is normal to the substrate. The edge-on orientation deducted from the π* dichroism is consistent with the standing up orientation deduced from the σ* dichroism. The exact orientation of the pentacene molecule in this particular film was quantified by integrating the π* intensity from 283 eV to 286.5 eV. Figure 3.8b plots that intensity versus $\sin^2 \theta$. A detailed analysis [11] quantified the extent of edge-on ordering in this sample by deriving a dichroic ratio, R given by

$$R = \frac{I(90^\circ) - I(0^\circ)}{I(90^\circ) + I(0^\circ)} \tag{3.6}$$

with the 0° and 90° values obtained by extrapolation from the intensities at the seven angles measured. In this approach to quantifying NEXAFS linear dichroism, $R = +1$ if the final orbital lies in the plane of the substrate, $R = 0$ when the final orbital is oriented at the magic angle ($\theta = 54.7°$), and $R = -1$ for an orbital aligned perpendicular to the substrate [11]. The analysis yielded an R value of 0.59(1) which indicates the pentacene molecules are strongly oriented in an edge-on fashion and the distribution of the molecular orientation is narrow. This was actually a result of significance to the goal of the study. When pentacene films of this type are used in OTFT, an edge-on orientation enhances π interactions in the source-drain plane, explaining the excellent high hole mobility when the pentacene molecules are properly oriented relative to the interface. In order to further optimize such devices NEXAFS was used to measure pentacene orientation as a function of film thickness, substrate chemistry, and substrate temperature. In other studies of pentacene, C 1s NEXAFS microscopy (STXM) has been used to map in-plane grain orientation based on the C 1s NEXAFS polarization dependence [67].

3.5 Examples

3.5.1 Pure polymeric materials

3.5.1.1 Fused aromatic rings

In the case of polymers with an aliphatic CH–CH backbone and pendant groups (e.g., polystyrene) bonds, there is little electronic interaction between repeat units, and the spectra are independent of chain length, except for very short oligomers. However, when there is extensive delocalization across repeat units (as is important in conducting polymers) the NEXAFS spectra can be strongly dependent on electronic interactions among adjacent units. Figure 3.9a shows how the C 1s → π* region (283–287 eV)

of the NEXAFS spectra of a series of fused phenyl rings evolves as the length of the fused ring system grows [68]. The delocalization of the π* orbitals across the full structure (Fig. 3.9b) leads to splittings which push the π* bands as low as 283.4 eV and as high as 286.2 eV, which is a much larger energy range than found for noninteracting phenyl groups. The complex pattern in these spectra, detected with a very high-resolution spectrometer ($E/\Delta E > 14{,}000$), is due to a combination of electronic level spitting and C–H and C–C vibrational excitation accompanying the C 1s excitation. While the details are beyond the scope of this chapter, it is noteworthy that

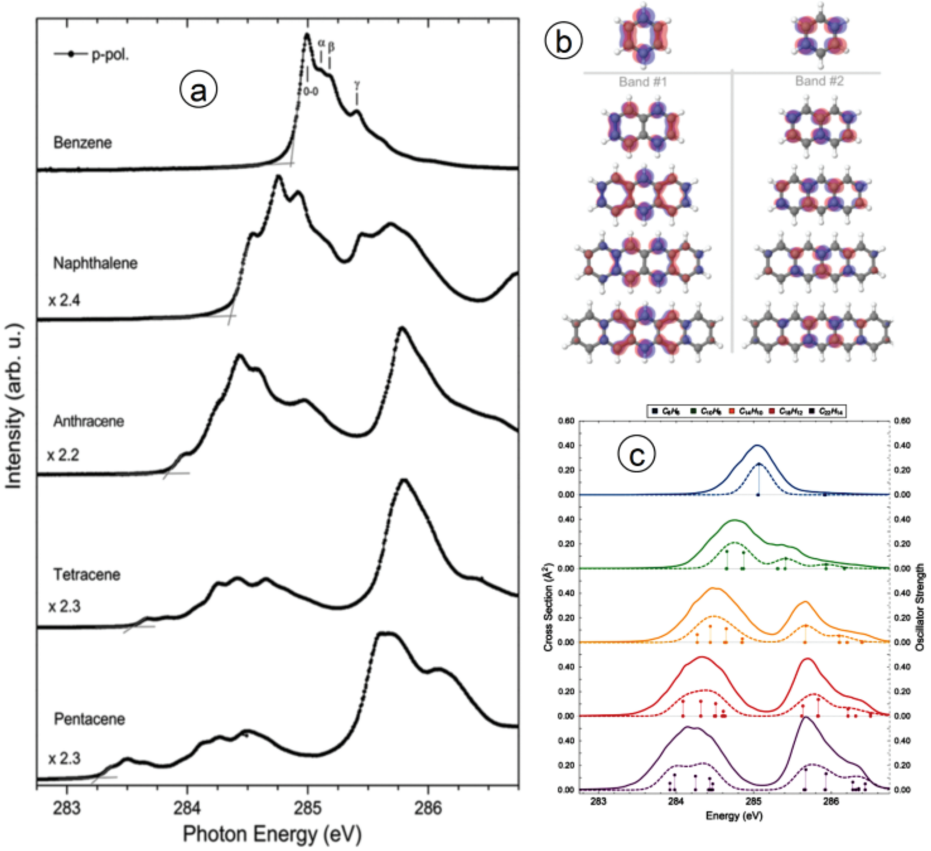

Fig. 3.9: Development of π* band structure of fused ring polyacenes [68]. (a) High-resolution C 1s NEXAFS of benzene, naphthalene, anthracene, tetracene and pentacene in the region of the C 1s → π* transitions. The fine structure is a combination of electronic and vibrational excitations. (b) Dominant band 1 and band 2π* molecular orbitals for naphthalene, anthracene, tetracene, and pentacene, related to the 1π* and 2π* of benzene. (c) Results of high-level density functional theory (DFT) calculations of these spectra. The vertical lines indicate positions of the π*electronic transitions (fixed ground state geometry), the dashed curves consider only electronic processes, while the full curves include consideration of vibrational excitations (adapted with permission from figs. 1–3 of [68]. Copyright 2018, American Chemical Society).

many of the spectral features arising from electronic interactions, nuclear motion and core hole effects were predicted with reasonable accuracy using DFT (Fig. 3.9b, c) [68]. The major deficiency of the computational aspect of this study, the over prediction of the intensity of the first band (283–285 eV) was attributed to insufficient treatment of the relaxation in the presence of the core hole. The authors speculated that using other functionals or using independent parameters for short- and long-range electronic interactions could remedy this deficiency [68].

3.5.1.2 Polysaccharides

Polysaccharides are biopolymers important in many aspects of biology and biotechnology. A NEXAFS study of eight different saccharides and polysaccharides [69] showed that fine details of the C 1s spectra could be used to differentiate each species (Fig. 3.10a). Further, with the support of FEFF8 multiple scattering calculations

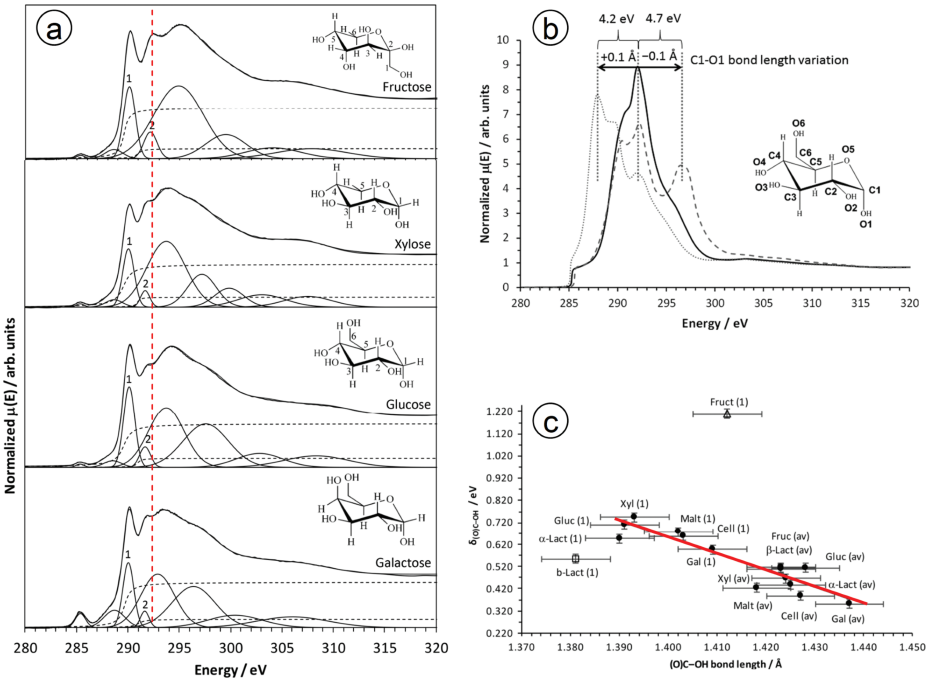

Fig. 3.10: C 1s NEXAFS of saccharides and polysaccharides[69]. (a) C 1s spectra of fructose, xylose, glucose and galactose, curve fit using Athena. Peak 1 is assigned to C 1s(C_1) → σ^*_{C-OH} and peak 2 is assigned to C 1s(C_1) → $\sigma^*_{(O)C-OH}$ transitions. (b) Feff8 simulation of the spectrum of the C_1 carbon of glucose, at the correct structure, and with +10 pm and –10 pm shifts of the C_1–OH bond length. (c) Linear correlation between the term value of the C 1s(C_1) → $\sigma^*_{(O)C-OH}$ transition and the C_1–OH bond lengths (adapted from figs. 1, 4, and 5 of [69], Creative Commons).

[70] of equilibrium and distorted structures of glucose (Fig. 3.10b), it was shown that the term value of the C 1s (C_1) → $\sigma^*_{(O)C-OH}$ transition – the difference in energy of the ionization potential for the C_1 carbon and the energy of peak 2 around 292 eV (Fig. 3.10a) – correlated with the length of the C–OH bond at the hemiacetal/hemiketal position (Fig. 3.10c). This type of bond length – term value correlation, first reported in 1984 [57], works well for bond lengths in small molecules constructed from second row atoms. This is one of the most subtle examples of this type of structure–spectral correlation to my knowledge. The high quality of the spectral peak fitting using Athena [71, 72] software was critical to this analysis. Athena is an important processing tool for NEXAFS data.

3.5.2 Surface versus bulk chain orientation

NEXAFS has been used to study the orientation of pendant groups at the surface of homopolymers. For example, Lenhart et al. [51] showed that there was a net alignment of phenyl groups normal to the exposed surface of various types of polystyrene, but that there is a wide range of tilt angles, particularly in more bulky substituted phenyl polystyrenes. A nice example of using NEXAFS to study molecular orientation of the bulk and surface of a complex polymer has been reported by Schuettfort et al. [73] These results are summarized in Fig. 3.11. The polymer studied was poly(*N*,*N*-bis-2-octyldodecylnaphthalene-1,4,5,8-bis-dicarboximide-2,6-diyl-alt5,5–2,2-bithiophene) [p(NDI2OD-T2)], a high-mobility conjugated polymer used in organic field-effect transistors (OFET). It was spun cast from a dilute aqueous solution on to a Si wafer (which established the chain orientation), and then floated off to form a free standing ~ 55 nm thin film. High surface-sensitive analysis is critical in this application since charge transport in the OFET occurs along a ~1 nm thick layer at the semiconductor/ polymer interface. Figure 3.11a defines the set of angles needed to describe the orientation of the polymer chains at the surface while Fig. 3.11b shows how the Auger electron yield (AEY), total electron yield (TEY) and transmission C 1s NEXAFS spectra were measured simultaneously. By comparing the polar angle dependence of the AEY, TEY and transmission C 1s NEXAFS spectra (Fig. 3.11c), they showed that the surface layer of the solvent cast p(NDI2OD-T2) film had a significantly smaller tilt angle (41°) than the bulk of the polymer (55°) (Fig. 3.11d). Further they measured the azimuthal angle dependence of the C 1s spectra of as-cast and melt-annealed p(NDI2OD-T2) films and showed that the polar and azimuthal alignment of the molecular units at the surface was the same in both preparations. In contrast, the molecular orientation in the bulk differed significantly (see Fig. 3.11e). The NEXAFS results [73] provided a consistent microstructural explanation of bulk and surface charge transport phenomena previously observed in p(NDI2OD-T2) films. In particular, the observation of a distinct edge-on surface orientation in spin-coated P(NDI2OD-T2) accounts for the high-charge transport mobilities observed in top-gate transistors. As part of this study, the same

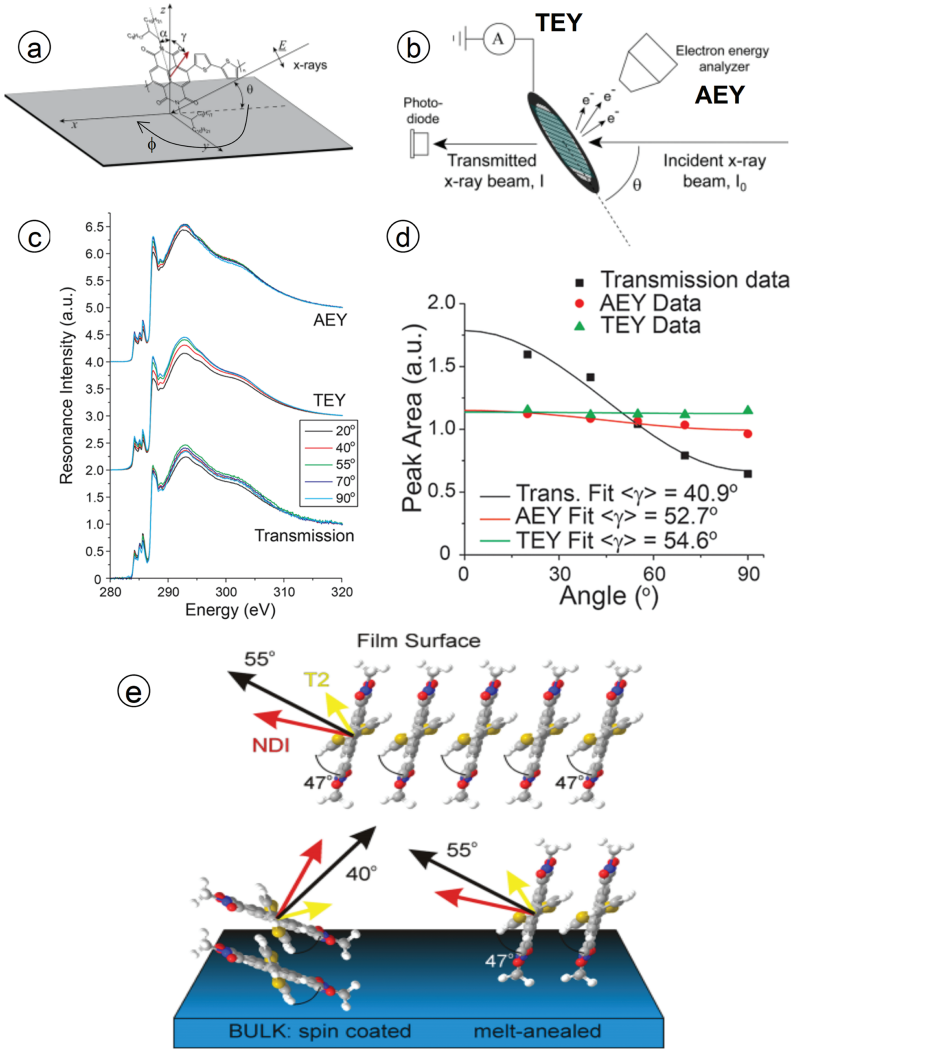

Fig. 3.11: Using angle-resolved NEXAFS to deduce surface versus bulk orientation of P(NDI2OD-T2), an organic field-effect transistor material [73]. (a) Schematic defining the experimental geometry and the polar (θ) and azimuthal (ϕ) angles, for which the polarization dependence was measured. The arrow perpendicular to the molecular plane indicates the dipole transition dipole moment (TDM). (b) Experimental geometry used to simultaneously measure total electron yield (TEY), Auger electron yield (AEY), and transmission signals. (c) Polar angle-resolved AEY, TEY, and transmission NEXAFS spectra of the as-cast P(NDI2OD-T2) film. (d) Polar angle dependence of the 1s → π* peak area for the three different types of spectra. (e) Cartoon of molecular orientation at the surface and bulk based on the measured values of the overall TDM (black arrow). The deduced orientation of the individual naphthalene diimide (NDI, red) and thiophene (T2, yellow) units relative to the TDM are indicated for a dihedral angle of 47°. Only the NDI and T2 cores are shown (adapted with permission from [73] . Copyright 2013, American Chemical Society).

samples were also measured by grazing incidence wide-angle X-ray scattering (GIWAXS) [73]. However, GIWAXS was unable to differentiate the surface and bulk structure, due to its much larger sampling depth than AEY- or TEY-NEXAFS.

3.6 Spectromicroscopy of polymers

C 1s NEXAFS spectromicroscopy has proven to be of tremendous value in many studies of both the bulk and surface of homogeneous and heterogeneous polymers since the capability was first demonstrated by Ade et al. [12]. Because polymers such as Kevlar exhibit strong molecular alignment, one can use the difference in x-ray absorption between spectra recorded with linear polarization in two (ideally orthogonal) directions to characterize the polymer orientation in the plane of the thin section [74]. A wide variety of multicomponent polymer materials have been studied using implementations of NEXAFS in soft X-ray microscopes. Several reviews of soft X-ray NEXAFS microscopy have been published [17, 18, 75, 76]. C 1s NEXAFS microscopy has been applied to a large number of polymer types [20, 21, 25]. A bibliography of the soft X-ray microscopy literature can be accessed at http://unicorn.mcmaster.ca/xrm-biblio/xrm_bib.html. Two major soft X-ray spectromicroscopy techniques have been applied to polymer surfaces: X-ray photoemission electron microscopy (X-PEEM) and scanning transmission X-ray microscopy (STXM). Here these two NEXAFS microscopies are described, and examples of their application to adsorption of proteins to polymeric biomaterial surfaces are given.

3.6.1 NEXAFS microscopy methods

3.6.1.1 X-ray photoemission electron microscopy (XPEEM)

XPEEM [77] is a full-field microscopy in which a lateral area (2–60 μm) of a surface is illuminated by monochromatic X-rays (Fig. 3.12a). Electrons created near the surface are ejected and accelerated by an electric field (<1 kV/mm) into an electrostatic or magnetic electron microscope column to make a magnified image. The image is detected by a suitable imaging system, typically a channel plate to amplify the electron signal, a phosphor to convert electron pulses to visible light, followed by a digital camera (Fig. 3.12a). XPEEM instruments are housed in ultrahigh vacuum (UHV) chambers ($P < 10^{-9}$ mbar) so polymer films which outgas cannot be studied. NEXAFS spectroscopy and NEXAFS imaging are obtained by measuring sequences of XPEEM images over a range of X-ray energies. Due to the high field at the surface and the high sensitivity of the XPEEM analyzer to secondary electrons, the sampling depth is somewhat larger than typical TEY sampling depths, of the order of 10 nm

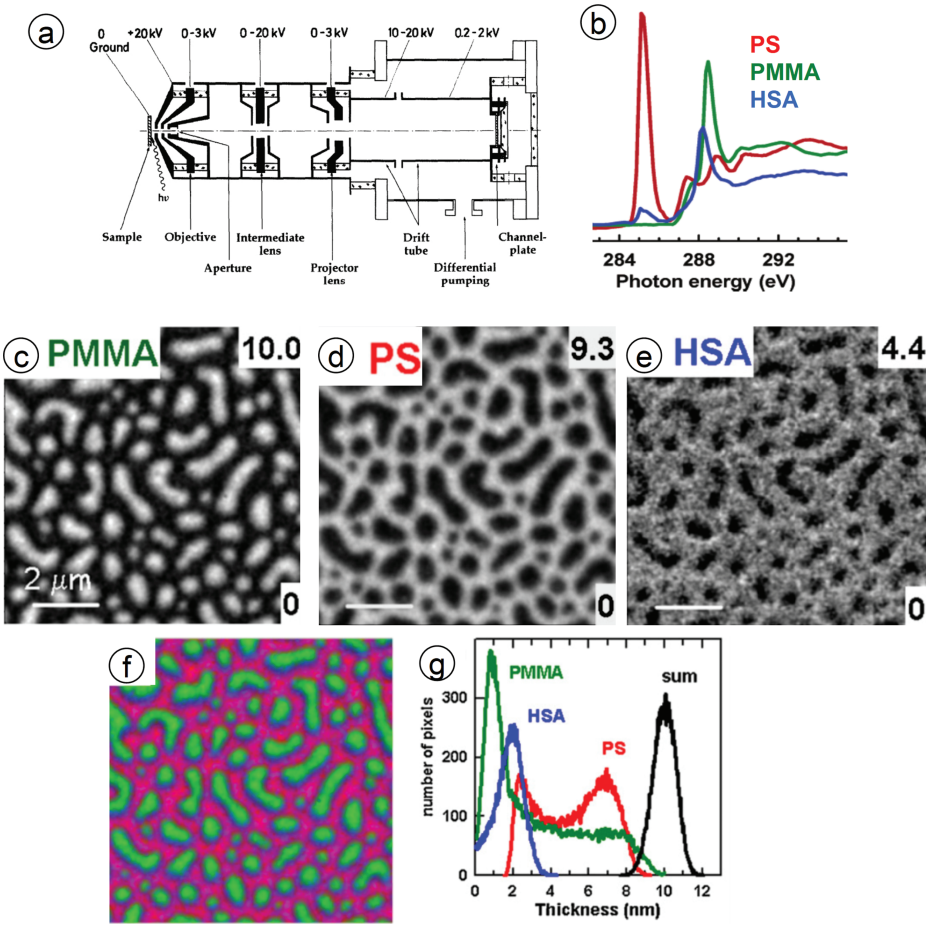

Fig. 3.12: XPEEM visualization of the adsorption of human serum albumin (HSA) on a spun-cast phase-segregated polystyrene/polymethylmethacrylate (PS/PMMA) surface [7, 80]. (a) Schematic of an X-ray photoemission electron microscope (XPEEM).(b) C 1s spectra of PS, PMMA and HSA. Maps of (c) PMMA, (d) PS, and (c) HSA in the single domain thick film. (f) Rescaled color-coded composite of the PMMA (green), PS (red), and HSA (blue) component maps. (g) Histograms of the thickness distributions of the three components. The sum of the gray scales of the three components has been normalized to 10 nm, a sampling depth determined experimentally (from [80], used with permission).

[42]. There are significant challenges to applying XPEEM to polymer surfaces, including sample charging, UHV vacuum incompatibility, radiation damage [48], and sample damage by arcing caused by the high field at the surface. However, with thin samples (<50 nm), rapid shuttering, short exposures, and careful control of total exposure times, XPEEEM has been applied successfully to a number of polymer surfaces, including environmentally responsive polymer brush surfaces [78],

and candidate biomaterials [79]. An example from a study of protein adsorption on a polymer blend is given below. In other studies, XPEEM has been used to investigate competitive adsorption of peptides versus proteins [80] and pH-responsive surfaces [81].

3.6.1.2 Scanning transmission X-ray microscopy (STXM)

In STXM [18, 29, 75, 76] a Fresnel zone plate (ZP) is used to create a finely focused (<30 nm spot size) monochromated X-ray beam. A sample with partial X-ray transmission at the core level of interest is placed at the ZP focal point and (x, y) raster scanned while recording the transmitted X-ray intensity (see Fig. 3.13a). Images constructed from the transmitted intensity are recorded over a range of photon energies, and converted to OD using an I_o signal measured by STXM through a path that includes all except the sample. Since STXM is a type of X-ray in, X-ray out technique, the vacuum requirements are not very stringent, such that measurements can be made at 1 bar He, reduced pressure with saturated water vapor, and on fully hydrated samples with up to 3 μm thick aqueous layer. This flexibility has lead to STXM being used frequently for *operando* or in situ studies of materials, including polymers [82]. Electron yield detection can be used and comparisons have been made of bulk properties, probed by transmission, and surface properties, probed by TEY [83]. Here, in order to compare XPEEM and STXM applied to a similar problem, Section 3.7.3 presents results from visualization of the selective adsorption of a protein at the complex surface of a polyurethane polymer containing two types of reinforcing particles [77].

3.6.2 XPEEM of protein adsorption on PS/PMMA

Many polymer materials are used in medical technology. Frequently, it is desirable to optimize the innate or modified surface chemistry and morphology for specific medical applications. Characterization of the surfaces of such biomaterials and quantitative evaluation of their interaction with relevant proteins, peptides, and other biologically active species is an important part of biomaterials optimization. The goal of imaging polymeric biomaterial surfaces is to determine and understand the chemical and morphological factors which improve biocompatibility. In general, proteins or peptides are the first species to adsorb to biomaterials and thus much of biomaterials optimization involves controlling protein–surface interactions. In this context control may refer to complete prevention or minimization of adsorption (protein resistance and antifouling), or it may refer to the selective promotion of adsorption of one specific protein from the complex mix of species present in a biological tissue or fluid with which the biomaterial is in contact. Thus, studies in which the competition for adsorption by

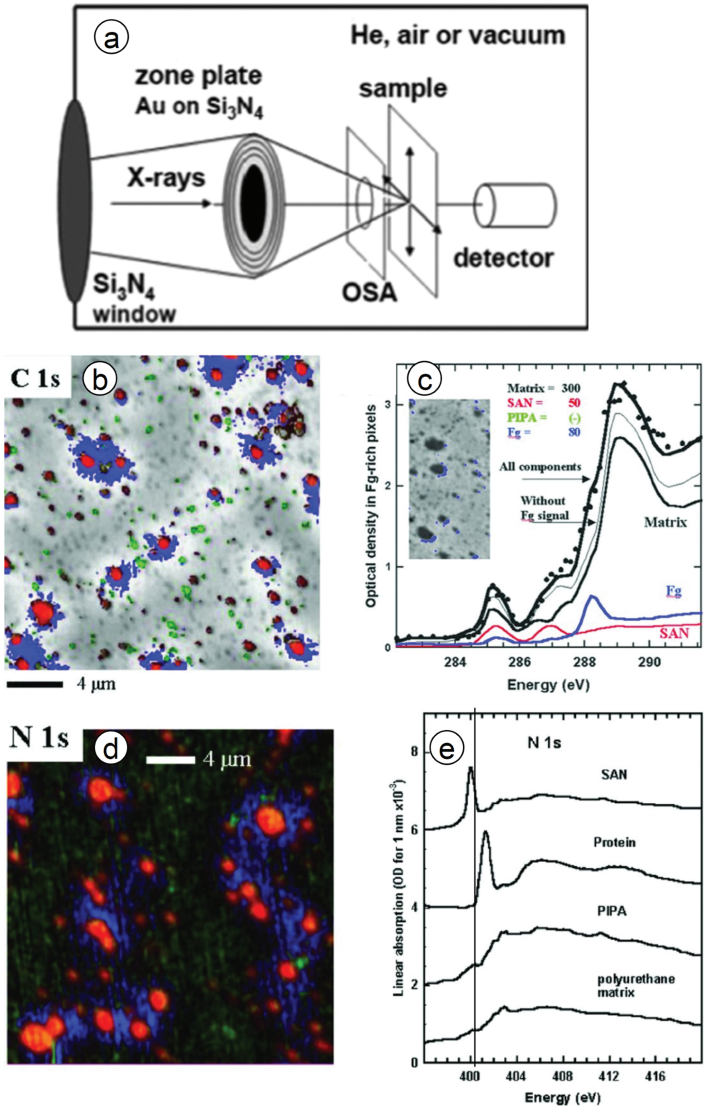

Fig. 3.13: STXM mapping of the adsorption of fibrinogen (Fg) on a polyurethane (matrix) with reinforcing styrene acrylonitrile (SAN) and poly-isocyanate polyaddition product (PIPA) particles [84]. (a) Schematic of a scanning transmission X-ray microscope (STXM). (b) Rescaled color-coded composite of the four-component maps derived from a C 1s image sequence – polyurethane matrix (gray scale); SAN (red); PIPA (green); Fg (blue). (c) Curve fit analysis of the C 1s spectrum of the pixels identified as having large Fg content. The thick line, which is a good match to the data (points), includes the Fg component in the fit, while the thin line, excludes Fg from the fit. The insert shows the pixels selected (Fg in blue on the grayscale polyurethane). (d) Rescaled color-coded composite of SAN (red), PIPA (green), and Fg (blue) distributions derived by fitting an N 1s image sequence. (e) N 1s spectra of the SAN, Fg, PIPA, and polyurethane spectra, used in the fit (from [84], used with permission).

several species to the same surface is studied by chemically sensitive surface imaging are of interest.

Figure 3.12 presents results from an XPEEM study of a 0.005 mg/mL aqueous solution of human serum albumin (HSA), interacted for 20 min with the surface of a phase segregated 30 wt% polystyrene/70 wt% polymethyl methacrylate (PS/PMMA) blend [80]. The surface was thoroughly rinsed and then placed directly into the load lock chamber, and pumped for ~20 min to dry it. Figure 3.12b presents the C 1s NEXAFS spectra of the three species on a comparable absolute intensity scale, showing they can be easily differentiated. These reference spectra were used to fit a C 1s image stack measured by XPEEM and thus derive maps of the surface distribution of the three species. The sampling depth was measured to be 10 nm [80]. The ~ 50 nm thick polymer blend film was prepared by spin-coating dilute toluene solutions of the indicated composition on to native oxide silicon wafers. This polymer blend surface, which has been studied extensively by both XPEEM [79–81] and STXM [84–87] naturally phase segregates to produce isolated 0.5–2 μm sized PMMA domains (Fig. 3.12c) in a continuous PS domain (Fig. 3.12d). The fact that the minority species is the continuous domain is surprising. This is believed to be due to preferential attraction of the PMMA to the hydrophilic oxidized silicon substrate [88], although other factors, such as the higher surface activity of PS [89], may also play a role. This blend surface is an interesting candidate for competitive adsorption studies since the PS domain is strongly hydrophobic, the PMMA domains are quite hydrophilic, and the interphase, a region of 10–30 nm at the boundary of the PS and PMMA domains has both characteristics. Figure 3.12e presents a map of the signal from HSA on the PS/PMMA surface, derived from a three-component fit to a C 1s image sequence [80]. Comparison of the maps of HSA and PS suggests that the protein prefers to adsorb to the hydrophobic PS domain. However, the color-coded composition of the three maps (Fig. 3.12f) shows there is a clear preference to the PS–PMMA interphase. HSA is an amphiphilic protein, with both hydrophobic and hydrophilic regions at its surface, so the interphase offers more opportunities for strong binding. In addition to mapping of HSA on PS/PMMA, competitive adsorption of HSA and SUB-6, an antimicrobial peptide, to the PS/PMMA surface was also measured [80].

3.6.3 STXM of protein (Fg) adsorption on a reinforced polyurethane

Polyurethanes (PU) are commonly used in medical applications due to their favorable mechanical and chemical properties. The adsorption of fibrinogen (Fg) to a complex multicomponent polyurethane thin film in which the polyether-rich toluene-di-isocyante (TDI) polyurethane matrix was reinforced with styrene-b-acrylonitrile (SAN) particles and poly-isocyanate poly-addition product (PIPA, a methylene diphenyl diisocyanate (MDI)-based hard segment-like material) particles. A STXM

study of the chemistry and morphology of the polyurethane [90, 91] showed the SAN and PIPA particles could be readily differentiated from their NEXAFS signals. The lateral distribution of the Fg protein on the TDI-PU_SAN_PIPA surface was determined by STXM [84] for three types of samples: (i) Fg exposure from phosphate buffer solution, followed by rigorous rinsing with buffer, then dried. (ii) the same protocol but using exposure to a pure aqueous overlayer, followed by rinsing and drying. (iii) an in situ study in which the polyurethane film covered by ~ 1 μm of dilute protein solution trapped between two silicon nitride windows. Figure 3.13 presents results from a C 1s and N 1s STXM study of the in situ sample [84]. Both the C 1s (Fig. 3.13b,c) and N 1s (Fig. 3.13d,e) results show that Fg prefers to adsorb to regions of the matrix at the edges of the larger SAN particles. While the C 1s analysis was quite subtle, and required careful peak fitting analysis (Fig. 3.13c), the N 1s edge was particularly informative, since protein has many N atoms and a characteristic spectrum. While the SAN particles also have significant amounts of nitrogen, the N 1s $\rightarrow\pi^*_{\text{nitrile}}$ transition (399.8 eV) is easily distinguished from the N 1s $\rightarrow\pi^*_{\text{amide}}$ transition (401.2 eV) (see Fig. 3.13e). Figure 3.13d shows a color-coded composite derived from a N 1s image sequence. A similar conclusion as to preferred adsorption site was reached for the ex situ Fg exposed sample measured after rinsing and drying. While the detailed mechanism of Fg adsorption to the SAN–polyurethane interface is not clear, surface topography may be playing a role since the SAN particles protrude up to 50 nm from the surface.

3.7 Summary

From a purely spectroscopy perspective, there is ample flux at existing synchrotron facilities to apply NEXAFS spectroscopy to most polymer science problems where the sample is unchanging or only changing on a second or slower timescale. Radiation damage is a significant limitation for NEXAFS microscopy of many polymers, particularly fluorinated species such as perfluorosulfonic acid (PFSA) ionomer [48, 92, 93]. However, if an unfocused or intentionally defocused beam is used, the dose can be reduced to the point where radiation damage is not a problem, of course, at the expense of spatial resolution. At this time, a revolution happening in synchrotron sources improves the flux and brightness of the monochromated X-rays [94]. These two to three orders of magnitude improvement will make NEXAFS spectroscopy and microscopy significantly more powerful. For purely spectroscopic applications, the new fourth-generation light sources will be able to follow the kinetics and dynamics of chemical and physical transformations of polymer surfaces [33, 82, 95–97]. As an example, the surface structure of hydrated polymers used as bioscaffolds for artificial tissue is known to be important to the success of tissue growth [98]. Static, ex situ approaches are giving insights [79] but the ability to follow the surface re-organization

and watch the tissue formation in real time is probably within the capabilities of NEXAFS spectroscopy at fourth-generation light sources. In addition to improving "conventional" STXM, the much higher brightness will make dramatic improvements to the newly emerging method of soft X-ray ptychography which already is providing spatial resolutions below 10 nm [99, 100]. It is expected, once systems are fully optimized, the spatial resolution will routinely be limited only by wavelength of the X-rays (~4 nm at the C 1s edge). This is almost the case for the dedicated COSMIC ptychography system at the Advanced Light source (Berkeley, CA, USA) [100]. As an example, F 1s ptychography has been used to map PFSA ionomer in the membrane electrode assembly of polymer electrolyte membrane fuel cells (PEM-FC) with a resolution better than 15 nm in 2D and 30 nm in 3D [101]. In general, in situ and *operando* studies of polymer surfaces are emerging as an increasingly important application of NEXAFS. The future of NEXAFS, as a tool to study both bulk and surface properties of polymers, is very bright indeed!

References

[1] Rubensson J-E. Synchrotron Radiation: An everyday application of special relativity. IOP Concise Phys 2016.
[2] Hanawalt JD. The dependence of x-ray absorption spectra upon chemical and physical state. J D Phys Rev 1931, 37, 715–726.
[3] Röntgen WC. Uber eine neue art von strahlen.I Mitteilung. Sitzungs-Berichtedel Physikalisch-medicinischen Gesellshaft Zu Würzburg 1895, 137, 132–141.
[4] Brion CE, Daviel S, Sodhi R, Hitchcock AP Recent advances in inner-shell excitation of free molecules by electron energy loss spectroscopy, AIP Conference Proceedings 1982;92:429–446.
[5] Koch EE, Sonntag BF. Molecular spectroscopy. In: Kunz C, ed. Synchrotron Radiation Techniques and Applications, Berlin, Springer, Topics Curr Phys, 1979, 10.269-355.
[6] Chen CT, Sette F. Performance of the Dragon soft x-ray beamline. Rev Sci Instr 1998, 60, 1616–1621.
[7] Stöhr J. NEXAFS Spectroscopy, Springer Ser Surf Sci, Vol. 25, Springer,, 1992.
[8] Stöhr J, Outka DA. Determination of molecular orientations on surfaces from the angular dependence of near-edge x-ray-absorption fine-structure spectra. Phys Rev B 1987, 36, 7891–7905.
[9] Jordan-Sweet JL, Kovac CA, Goldberg MJ, Morar JF. Polymer/metal interfaces studied by carbon near-edge x-ray absorption fine structure spectroscopy. J Chem Phys 1988, 89, 2482–2489.
[10] Outka DA, Stöhr J, Rabe JP, Swalen JD. The orientation of Langmuir–Blodgett monolayers using NEXAFS. J Chem Phys 1988, 88, 4076–4087.
[11] DeLongchamp D, Lin EK, Fischer DA. Organic semiconductor structure and chemistry from near-edge x-ray absorption fine structure (NEXAFS) Spectroscopy. Proc SPIE Organic Field-Effect Transistors IV 2005, 5940:59400A.
[12] Ade H, Zhang X, Cameron S, Costello C, Kirz J, Williams S. Chemical contrast in X-ray microscopy and spatially resolved XANES spectroscopy of organic specimens. Science 1992, 258, 972–975.

[13] 1Hähner G. Near edge X-ray absorption fine structure spectroscopy as a tool to probe electronic and structural properties of thin organic films and liquids. Chem Soc Rev 2006, 35, 1244–1255.
[14] DeLongchamp DM, Kline RJ, Fischer DA, Richter LJ, Toney MF. Molecular characterization of organic electronic films. Adv Mater 2011, 23, 319–337.
[15] Watts B, Thomsen L, Dastoor PC. Methods in carbon K-edge NEXAFS: Experiment and analysis. J Electron Spectrosc Rel Phenom 2006, 151, 105–120.
[16] Unger WES, Lippitz A, Wöll C, Heckmann W. X-ray absorption spectroscopy (NEXAFS) of polymer surfaces. Fresenius J Anal Chem 1997, 358, 89–92.
[17] Ade H, Urquhart SG. NEXAFS spectroscopy and microscopy of natural and synthetic polymers, Chapter 4 of "Chemical applications of synchrotron radiation" (T.K. Sham, ed.) Part I: Dynamics and VUV Spectroscopy. In: Advanced Series in Physical Chemistry Vol 12A, Singapore, World Scientific, 2002, 154–227.
[18] Ade H, Hitchcock AP. NEXAFS microscopy and resonant scattering: Composition and orientation probed in real and reciprocal space. Polymer 2008, 49, 643–675.
[19] Son D, Cho S, Nam J, Lee H, Kim M. X-ray-Based spectroscopic techniques for characterization of polymer nanocomposite materials at a molecular level. Polymers 2020, 12, 1053.
[20] Dhez O, Ade H, Urquhart SG. Calibrated NEXAFS spectra of some common polymers. J El Spec Rel Phen 2003, 128, 85–96.
[21] Urquhart SG, Hitchcock AP, Smith AP, et al. NEXAFS spectromicroscopy of polymers: Overview and quantitative analysis of polyurethane polymers. J Electron Spectrosc Rel Phenom 1999, 100, 119–135.
[22] Urquhart SG, Smith AP, Ade HW, Hitchcock AP, Rightor EG, Lidy W. Near-edge X-ray absorption fine structure spectroscopy of MDI and TDI polyurethane polymers. J Phys Chem B 1999, 103, 4603–4610.
[23] Urquhart SG, Hitchcock AP, Leapman RD, Priester RD, Rightor EG. Analysis of polyurethanes using core excitation spectroscopy. Part I: Model polyurethane foam polymers. J Polym Sci Part B: Polym Phys 1995, 33, 1593–1602.
[24] Urquhart SG, Hitchcock AP, Priester RD, Rightor EG. Analysis of polyurethanes using core excitation spectroscopy. Part II: Inner shell spectra of ether, urea and carbamate model compounds. J Polym Sci Part B: Polym Phys 1995, 33, 1603–1620.
[25] Smith AP, Urquhart SG, Winesett DA, Mitchell G, Ade H. Use of near edge x-ray absorption fine structure spectromicroscopy to characterize multicomponent polymeric systems. Appl Spectrosc 2001, 55, 1676–1681.
[26] Graf N, Yegen E, Gross T, et al. XPS and NEXAFS studies of aliphatic and aromatic amine species on functionalized surfaces. Surf Sci 2009, 603, 2849–2860.
[27] Watts B, Swaraj S, Nordlund D, Lüning J, Ade H. Calibrated NEXAFS spectra of common conjugated polymers. J Chem Phys 2011, 134, 024702.
[28] Henke BL, Gullikson EM, Davis JC. X-ray interactions: Photoabsorption, scattering, transmission, and reflection at E = 50-30,000 eV, Z = 1-92. At Data Nucl Data Tables 1993, 54, 181–342.
[29] Jacobsen C. X-ray Microscopy, Cambridge University Press, 2019.
[30] Guillemin R, Decleva P, Stener M, et al. Selecting core-hole localization or delocalization in CS_2 by photofragmentation dynamics. Nat Commun 2015, 6, 6166.
[31] Ishii I, Hitchcock AP. A Quantitative experimental study of the core excited electronic states in formamide, formic acid and formyl fluoride. J Chem Phys 1987, 87, 830–839.
[32] Wen AT, Ruehl E, Hitchcock AP. Inner-shell excitation of organoiron compounds by electron impact. Organometallics 1992, 11, 2559–2569.

[33] Su GM, Cordova IA, Brady MA, Prendergast D, Wang C. Combining theory and experiment for X-ray absorption spectroscopy and resonant X-ray scattering characterization of polymers. Polymer 2016, 99, 782–796.
[34] Su GM, Patel SN, Pemmaraju CD, Prendergast D, Chabinyc ML. First-principles predictions of near-edge x-ray absorption fine structure spectra of semiconducting polymers. J Phys Chem C 2017, 121, 9142–9152.
[35] Michelitsch GS, Reuter K. Efficient simulation of near-edge x-ray absorption fine structure (NEXAFS) in density-functional theory: Comparison of core-level constraining approaches. J Chem Phys 2019, 150, 074104.
[36] Kosugi N. Strategies to vectorize conventional SCF-Cl algorithms. Theoret Chim Acta 1987, 72, 149–173.
[37] Schöll A, Fink R, Umbach E, Mitchell GE, Urquhart SG, Ade H. Towards a detailed understanding of the NEXAFS spectra of bulk polyethylene copolymers and related alkanes. Chem Phys Lett 2003, 370, 834–841.
[38] Nagasaka M, Yuzawa H, Kosugi N. Intermolecular interactions of pyridine in liquid phase and aqueous solution studied by soft x-ray absorption spectroscopy. Zeitschrift Für Physikalische Chemie 2018, 232, 705–722.
[39] Zimmermann P, Peredkov S, Abdala PM, et al. Modern X-ray spectroscopy: XAS and XES in the laboratory. Coord Chem Rev 2020, 423, 213466.
[40] Lewis S, Gelb J, Sh L, Yun W, Vine D, Stripe B, Seshadri S. Recent Developments in laboratory x-ray microanalytical techniques for electronic structure, chemical composition, and microstructure of metals and materials. Microsc Microanal 2002, 26(S2), 516–516.
[41] Paroli B, Potenza MAC. Radiation emission processes and properties: Synchrotron, undulator and betatron radiation. Adv Phys X 2017, 2, 978–1004.
[42] Wolfgang Grünert and Konstantin Klementiev, X-ray absorption spectroscopy principles and practical use in materials analysis, De Gruyter, (accessed: March 5, 2020 at https://doi.org/10.1515/psr-2017-0181)
[43] Dohlus M, Rossbach J, Bethge KHW, et al. Application of accelerators and storage rings. In: Myers S, Schopper H, eds. Particle Physics Reference Library : Volume 3: Accelerators and Colliders, Springer International Publishing, 2020, 661–795.
[44] Kaznacheyev KV, Karunakaran C, He F, Sigrist M, Summers T, Obst M, Hitchcock AP. CLS ID-10 chicane configuration: From “simple” sharing to extended performance with high speed polarization switching. Nucl Inst Meth A 2007, 582, 103–106.
[45] Gann E, Crofts T, Holland G, et al A NIST facility for resonant soft x-ray scattering measuring nano-scale soft matter structure at NSLS-II. J Phys: Condens Matter 2021, 33, 164001.
[46] Hanhan S, Smith AM, Obst M, Hitchcock AP. Optimization of analysis of Ca 2p soft X-ray spectromicroscopy. J Electron Spectrosc Rel Phenom 2009, 173, 44–49.
[47] Gergely G, Menyhard M, Sulyok A, et al. Evaluation of the inelastic mean free path (IMFP) of electrons in polyaniline and polyacetylene samples obtained from elastic peak electron spectroscopy (EPES). Central Eur J Phys 2007, 5, 188–200.
[48] Wang J, Morin C, Li L, Hitchcock AP, Scholl A, Doran A. Radiation damage in soft X-ray microscopy. J El Spec Rel Phen 2009, 170, 25–36.
[49] Aygül U, Batchelor D, Dettinger U, et al. Molecular orientation in polymer films for organic solar cells studied by NEXAFS. J Phys Chem C 2012, 116, 4870–4874.
[50] Wu W, Sambasivan S, Wang C-Y, Wallace WE, Genzer J, Fischer DA. A direct comparison of surface and bulk chain-relaxation in polystyrene. Eur Phys J E 2003, 12, 127–132.

[51] Lenhart JL, Fischer DA, Chantawansri TL, Andzelm JW. Surface orientation of polystyrene based polymers: Steric effects from pendant groups on the phenyl ring. Langmuir 2012, 28, 15713–15724.
[52] Tamenori Y, Morita M, Nakamura T. Two-dimensional approach to fluorescence yield XANES measurement using a silicon drift detector. J Syn Rad 2011, 18, 747–752.
[53] Asakura D, Hosono E, Nanba Y, et al. Material/element-dependent fluorescence-yield modes on soft X-ray absorption spectroscopy of cathode materials for Li-ion batteries. AIP Adv 2016, 6, 035105.
[54] Chiang Y-J, Huang W-C, Ni C-K, Liu C-L, Tsai -C-C, Hu W-P. NEXAFS spectra and specific dissociation of oligo-peptide model molecules. AIP Adv 2019, 9, 085023.
[55] Ikeura-Sekiguchi H, Sekiguchi T, Baba Y, Imamura M, Matsubayashi N, Shimada H. Direct and indirect processes in photon-stimulated ion desorption from condensed formamide. Surf Sci 2005, 593, 303–309.
[56] Tardio S, Cumpson PJ. Practical estimation of XPS binding energies using widely available quantum chemistry software. Surface & Interface Analy 2018, 50, 5–12.
[57] Sette F, Stöhr J, Hitchcock AP. Determination of intramolecular bond lengths in gas phase molecules from K shell shape resonances. J Chem Phys 1984, 81, 4906–4914.
[58] Cooper G, Gordon M, Tulumello D, Turci C, Kaznatcheev K, Hitchcock AP. Inner shell excitation of glycine, glycyl-glycine, alanine and phenylalanine. J Electron Spectros Relat Phenomena 2004, 137–140, 795–799.
[59] Urquhart S, Ade H. Trends in the carbonyl core (C 1s, O 1s) → $\pi^*_{C=O}$ transition in the near-edge x-ray absorption fine structure spectra of organic molecules. J Phys Chem B 2002, 106, 8531–8538.
[60] Fu J, Urquhart SG. Linear dichroism in the X-ray absorption spectra of linear n-alkanes. J Phys Chem A 2005, 109, 11724–11732.
[61] Horsley JA, Stöhr J, Hitchcock AP, Newbury DC, Johnson AL, Sette F. Resonances in the K shell excitation spectra of benzene and pyridine: Gas phase, solid, and chemisorbed states. J Chem Phys 1998, 83, 6099.
[62] Liu AC, Stöhr J, Friend CM, Madix RJ. A critical interpretation of the near-edge X-ray absorption fine structure of chemisorbed benzene. Surf Sci 1990, 235, 107–115.
[63] Urquhart SG, Lanke U, Fu J. Characterization of molecular orientation in organic nanomaterials by X-ray linear dichroism. Int J Nanotech 2008, 5, 1138–1170.
[64] Nordén B. Applications of linear dichroism spectroscopy. Appl Spectrosc Rev 1978, 14, 157–248.
[65] Rodger A, Norden B. Circular Dichroism and Linear Dichroism, Oxford, U.K, Oxford University Press, 1997.
[66] Gamble LJ, Ravel B, Fischer DA, Castner DG. Surface structure and orientation of PTFE films determined by experimental and FEFF8-calculated NEXAFS spectra. Langmuir 2002, 18, 2183–2189.
[67] Bräuer B, Virkar A, Mannsfeld SCB, et al. X-ray microscopy imaging of the grain orientation in a pentacene field-effect transistor. Chem Mater 2010, 22, 3693–3697.
[68] Rocco MLM, Häming M, De Moura CEV, et al. High-resolution near-edge x-ray absorption fine structure study of condensed polyacenes. J Phys Chem C 2018, 122, 28692–28701.
[69] Gainar A, Stevens JS, Jaye C, Fischer DA, Schroeder SLM. NEXAFS sensitivity to bond lengths in complex molecular materials: A study of crystalline saccharides. J Phys Chem B 2015, 119, 14373–14381.
[70] Ankudinov AL, Ravel B, Rehr JJ, Conradson SD. Real-space multiple-scattering calculation and interpretation of x-ray-absorption near-edge structure. Phys Rev B 1998, 58, 7565–7576.

[71] Ravel B, Newville M. Athena, Artemis, Hephaestus: Data analysis for X-ray absorption spectroscopy using Ifeffit. J Synchrotron Radiat 2005, 12(Pt 4), 537–541.
[72] Ravel B, Newville M. Athena and Artemis: Interactive graphical data analysis using Ifeffit. Phys Scr 2005, T115, 1007.
[73] Schuettfort T, Thomsen L, McNeill CR. Observation of a distinct surface molecular orientation in films of a high mobility conjugated polymer. J Am Chem Soc 2013, 135, 1092–1101.
[74] Ade H, Hsiao B. X-ray linear dichroism microscopy. Science 1993, 262, 1427–1429.
[75] Hitchcock AP, Stöver HDH, Croll LM, Childs RF. Chemical mapping of polymer microstructure using soft x-ray spectromicroscopy. Aus J Chem 2005, 58, 423.
[76] Hitchcock AP. Soft X-ray imaging and spectromicroscopy Chapter 22. In: Tendeloo GV, Dyck DV, Pennycook SJ, eds. Handbook on Nanoscopy, Volume II, Wiley, 2012, 745–791.
[77] Anders S, Padmore HA, Duarte RM, et al. Photoemission electron microscope for the study of magnetic materials. Rev Sci Inst 1999, 70, 3973–3981.
[78] Li M, Pester CW. Mixed polymer brushes for "smart" surfaces. Polymers 2020, 12, 1553.
[79] Leung BO, Brash JL, Hitchcock AP. Characterization of biomaterials by soft x-ray spectromicroscopy. Materials (Basel) 2010, 3, 3911–3938.
[80] Leung BO, Hitchcock AP, Cornelius RM, Brash JL, Scholl A, Doran A. Using X-PEEM to study biomaterials: Protein and peptide adsorption to a polystyrene–poly(methyl methacrylate)-b-polyacrylic acid blend. J El Spec Rel Phen 2012, 185, 406–416.
[81] Hitchcock AP, Leung BO, Brash JL, Scholl A, Doran A. Soft X-ray spectromicroscopy of protein interactions with phase-segregated polymer surfaces. In: Proteins at Interfaces III State of the Art. Vol 1120. ACS Symposium Series.; 2012:731–760.
[82] Fink RH, Rosner B, Du X, et al. In-operando soft X-ray microspectroscopy of organic electronics devices. Microsc Microanal 2018, 24(S2), 424–425.
[83] Watts B, McNeill CR. Simultaneous surface and bulk imaging of polymer blends with X-ray spectromicroscopy. Macromol Rapid Commun 2010, 31, 1706–1712.
[84] Hitchcock AP, Morin C, Heng YM, Cornelius RM, Brash JL. Towards practical soft X-ray spectromicroscopy of biomaterials. J Biomater Sci, Polym Ed 2002, 13, 919–937.
[85] Morin C, Ikeura-Sekiguchi H, Tyliszczak T, et al. X-ray spectromicroscopy of immiscible polymer blends: Polystyrene–poly(methyl methacrylate). J Electron Spectros Relat Phenomena 2001, 121, 203–224.
[86] Li L, Hitchcock AP, Robar N, et al. X-ray microscopy studies of protein adsorption on a phase-segregated polystyrene/polymethyl methacrylate surface. 1. Concentration and exposure-time dependence for albumin adsorption. J Phys Chem B 2006, 110, 16763–16773.
[87] Li HAP, Cornelius R, Brash JL, Scholl A, Doran A. X-ray microscopy studies of protein adsorption on a phase segregated polystyrene/ polymethylmethacrylate surface. 2. Effect of pH on site preference. J Phys Chem B 2008, 112, 2150–2158.
[88] Harris M, Appel G, Ade H. Surface morphology of annealed polystyrene and poly(methyl methacrylate) thin film blends and bilayers. Macromolecules 2003, 36, 3307–3314.
[89] Winesett DA, Story S, Luning J, Ade H. Tuning substrate surface energies for blends of polystyrene and poly(methyl methacrylate). Langmuir 2003, 19, 8526–8535.
[90] Hitchcock AP, Koprinarov I, Tyliszczak T, et al. Optimization of scanning transmission X-ray microscopy for the identification and quantitation of reinforcing particles in polyurethanes. Ultramicroscopy 2001, 88, 33–49.
[91] Rightor EG, Urquhart SG, Hitchcock AP, et al. Identification and quantitation of urea precipitates in flexible polyurethane foam formulations by X-ray spectromicroscopy. Macromolecules 2002, 35, 5873–5882.
[92] Wu J, Melo LGA, Zhu X, et al. 4D imaging of polymer electrolyte membrane fuel cell catalyst layers by soft X-ray spectro-tomography. J Power Sources 2018, 381, 72–83.

[93] Martens I, Melo LGA, Wilkinson D, Bizzotto D, Hitchcock AP. Characterization of X-ray damage to perfluorosulfonic acid using correlative microscopy. J Phys Chem C 2019, 123, 16023–16033.
[94] Hitchcock AP, Toney MF. Spectromicroscopy and coherent diffraction imaging: Focus on energy materials applications. J Synchrotron Rad 2014, 21, 1019–1030.
[95] Liu Y, Russell TP, Samant MG, et al. Surface relaxations in polymers. Macromolecules 1997, 30, 7768–7771.
[96] Winter AD, Larios E, Alamgir FM, et al. Thermo-active behavior of ethylene-vinyl acetate / multiwall carbon nanotube composites examined by in situ near-edge x-ray absorption fine-structure spectroscopy. J Phys Chem C 2014, 118, 3733–3741.
[97] Winter AD, Czaniková K, Larios E, et al. Interface Dynamics in strained polymer nanocomposites: Stick–slip wrapping as a prelude to mechanical backbone twisting derived from sonication-induced amorphization. J Phys Chem C 2015, 119, 20091–20099.
[98] Dhandayuthapani B, Yoshida Y, Maekawa T, Kumar DS. Polymeric scaffolds in tissue engineering application: A review. Int J Polym Sci 2011, 2011, e290602.
[99] Stampanoni M, Menzel A, Watts B, Mader KS, Bunk O. Coherent x-ray imaging: Bridging the gap between atomic and micro-scale investigations. Chimia Int J Chem 2014, 6, 66–72.
[100] Shapiro DA, Babin S, Celestre RS, et al. An ultrahigh-resolution soft x-ray microscope for quantitative analysis of chemically heterogeneous nanomaterials. In: Science Advances, Vol. 6, 2020, eabc4904.
[101] Wu J, Zhu XH, West MM, et al. High resolution imaging of polymer electrolyte membrane fuel cell cathode layers by soft X-ray spectro-ptychography. J Phys Chem C 2018, 122, 11709–11719.
[102] Francis JT, Hitchcock AP. Inner-shell spectroscopy of p-benzoquinone, hydroquinone, and phenol: Distinguishing quinoid and benzenoid structures. J Phys Chem 1992, 96, 6598–6610.
[103] Francis JT, Hitchcock AP. Distinguishing keto and enol structures by inner-shell spectroscopy. J Phys Chem 1994, 98, 3650–3657.
[104] Scheinost AC, Kretzschmar R, Christ I, Jacobsen C. Carbon group chemistry of humic and fulvic acid: A comparison of C-1s NEXAFS and 1^3C-NMR spectroscopies. Chapter 9 in: Humic Substances: Structures. In:: Ghabbour EA, Davies G, eds. Models and Fnuctions, Cambridge, RSC, 2001, 39–48.
[105] Schumacher M, Christl I, Scheinost AC, Jacobsen C, Kretzschmar R. Chemical heterogeneity of organic soil colloids investigated by scanning transmission x-ray microscopy and C-1s NEXAFS microspectroscopy. Environ Sci Technol 2005, 39, 9094–9100.
[106] Schäfer T, Hertkorn N, Artinger R, Claret F, Bauer A. Functional group analysis of natural organic colloids and clay association kinetics using C(1s) spectromicroscopy. J Phys IV France 2003, 104, 409–412.